J. Fluid Mech. (1991), *vol.* 230, *pp.* 429–477
Printed in Great Britain

Frequency downshift in narrowbanded surface waves under the influence of wind

By TETSU HARA† AND CHIANG C. MEI
Department of Civil Engineering, Massachusetts Institute of Technology, Cambridge, MA 02139, USA

(Received 20 September 1990 and in revised form 27 February 1991)

It is well known that the spectral peak of wind-induced gravity waves on the sea surface tends to shift to lower frequencies as the fetch increases. In past theories the nonlinear dynamics subsequent to Benjamin–Feir instability has been found to initiate the downshift in narrow-banded waves in the absence of wind. However, these weakly nonlinear theories all predict the downshift to be only the first phase of an almost cyclic process. Limited by the length of a wave tank, existing experiments are usually made with relatively steep waves which often break. Although there is a theory on how breaking adds dissipation to stop the reversal of the initial trend of downshift, the details of breaking must be crudely characterized by semi-empirical hypotheses.

Since the direct role of wind itself must be relevant to the entire development of wind-wave spectrum, we examine here the effect of wind on the nonlinear evolution of unstable sidebands in narrow-banded waves. We assume that the waves do not break and consider the case where the nonlinear effects that initiate the downshift, energy input by wind and damping by internal dissipation all occur on the same timescale. This means that not only must the waves be mild but the wind stress intensity must also lie within a certain narrow range. With these limitations we couple the air flow above the waves with Dysthe's extension of the cubic Schrödinger equation, and examine the initial as well as the long-time evolution of a mechanically generated wavetrain. For a variety of wind intensities, downshift is indeed found to be enhanced and rendered long lasting.

1. Introduction

A well-known feature in the development of wind-wave spectra (e.g. Pierson, Neuman & James 1958; Hasselmann *et al.* 1973) is that as the fetch increases, the peak of the spectrum shifts to lower frequencies and increases in height, while the shape of the spectrum remains similar. It has been widely believed that this development is attributable to the combined effects of nonlinear wave interactions, input from the wind, and dissipation due to breaking. Much theoretical progress has been made by separately considering nonlinear interaction and wind-induced instability. The latter is, of course, the central topic in the theory of wind-wave generation. Breaking involves turbulence and air entrainment and is not yet amenable to thorough theoretical treatment.

With regard to nonlinear wave interactions, Lake *et al.* (1977) were the first to point out the relevance of the dynamic evolution subsequent to the Benjamin–Feir

† Current address: Woods Hole Oceanographic Institution, Woods Hole, MA 02543, USA.

instability. In particular, they observed in a wave tank that in the initial stage of unstable growth, the lower sideband grows at a faster rate than the upper sideband, while the carrier wave loses energy to levels lower than the sidebands. This unequal growth implies a tendency of downward shift of the spectral peak. They also suggested that breaking may be instrumental in protecting the downshift from disappearing as the spectrum tends to return to the original form. Later experiments by Melville (1982) for rather steep waves showed that breaking occurs when modulation is the greatest, i.e. when the lower sideband is at its peak, therefore rendering it impossible for the spectrum to reverse completely. Companion theories by Lake *et al.* showed that the cubic Schrödinger equation, which is valid for weak nonlinearity, can only predict equal growth rates of upper and lower sidebands, and that the spectrum tends to return to the original form periodically over a long timescale. Fuller theories based either on Zakharov's integral equation (Yuen & Lake 1982) or Dysthe's fourth-order extension to the Schrödinger equation (Dysthe 1979; Lo & Mei 1985) can predict the faster initial growth of the lower sideband. However, this asymmetry is only temporary, since the spectrum is modulated periodically and downshift occurs only when the modulation is greatest. Recently, Trulsen & Dysthe (1989) incorporated the effect of wave breaking to Dysthe's fourth-order equation, by introducing a heuristic and highly simplified criterion that all waves exceeding a certain height lose their energy. Their results indeed show a tendency of permanent frequency downshift, therefore supporting Lake *et al.* qualitatively. To incorporate all physical parameters quantitatively in this breaking model is however a formidable theoretical task.

So far there has been no theory on the joint effects of two elements that can be treated theoretically, i.e. nonlinear interaction and wind forcing; the only exception being Janssen (1986) on the period-doubling of gravity–capillary waves. Detailed experiments in a relatively short tank have been reported by Bliven, Huang & Long (1986) who focused their attention on the initial growth of sidebands for relatively steep waves and strong wind. For waves with initial steepness $ka = 0.22$ and wind intensity corresponding to $u'_*/C = 0.23-0.43$ (u'_* is the friction velocity and C is the phase speed), they found that, as u'_*/C increases, the sideband growth rate is reduced and that the separation between the sidebands widens, leading to a broader spectrum. However, for a milder initial slope $ka = 0.15$ the sideband growth rate is not significantly affected by wind. Li, Hui & Donelan (1987) described similar experiments and found that the sideband growth was suppressed by a strong wind but enhanced by a weak wind. Attributing this to the effect of wind-induced shear in water, they proposed an instability theory for modulated waves on a strong and linear shear current, and showed that the growth rate indeed increases with weak vorticity but decreases with high vorticity. However, the change in spectral band width as observed by Bliven *et al.* was not predicted. Moreover, the direct effects of wind stress on the water surface were not considered and the vorticity in the shear current was only prescribed but not derived. A fuller account of wind/water interaction is desirable.

In this paper, we shall examine theoretically how wind, blowing in the direction of wave propagation, affects the initial sideband instability of narrow-banded, long-crested waves, as well as their nonlinear dynamics at large time. In view of the results of Lo & Mei, it is necessary to include the fourth-order terms of Dysthe to initiate the asymmetric growth of sidebands.† Therefore we shall assume that the rate of energy

† Even within the third-order Schrödinger theory it is possible to impose an asymmetric initial condition artificially. The subsequent nonlinear evolution is then likely to remain asymmetric.

input by wind and the damping rate are also of fourth-order importance. These assumptions imply a weak wind within a narrow range of intensity. Without waves, the basic velocity profile in air is assumed to be linear in height near the water surface and logarithmic high above. The wave-induced turbulent disturbance is simply characterized by a constant eddy viscosity. Similar assumptions are made for water. The value of the empirical constant in the definition of the eddy viscosity is chosen so that the initial growth rate of waves matches existing experimental data.

After presenting the basic formulation in §3, we examine in §§4 and 5 the air flow over weakly nonlinear gravity waves. The air flow is computed numerically as in Caponi *et al.* (1982) for a laminar flow over a wave surface. Next, in §6 we derive the evolution equation of surface gravity waves up to the fourth order in wave steepness, including the effect of wind-induced current in water, the wind energy input, and the damping of waves due to eddy viscosity. The initial growth rate and the subsequent nonlinear evolution of the Benjamin–Feir instability are then examined in §§7 and 8. Tendency of frequency downshift at large time is discussed.

Mathematically a somewhat similar problem was treated by Blennerhassett (1980) who considered a two-layered fluid in a horizontal channel bounded above and below by solid walls. With the upper wall moving at a constant velocity horizontally, the sideband instability of the interface was studied by first deducing the evolution equation of the Schrödinger type. The densities of the two fluids were assumed to be comparable, and the flow laminar. Hence, the theory is not immediately related to the wind/wave problem. Recently Dhar & Das (1990) examined the initial growth rate of the Benjamin–Feir instability based on the fourth-order evolution equation of gravity waves in the presence of wind. They treated the wind as a potential flow and matched only the vertical velocity and the pressure at the interface. Therefore, their theory is relevant only to two perfect fluids.

2. Turbulence model for air flow and water motion

For air flow over infinitesimal waves various turbulence models have been proposed before (e.g. Townsend 1972). Recently Jacobs (1987) has re-examined this problem by using an eddy viscosity linearly varying in height above the waves, and has concluded that the energy input rate is insensitive to the turbulence model assumed. For a prescribed permanent wave with a small but finite wave slope the analysis is less simple. Only Gent & Taylor (1976) have solved the nonlinear equations of air flow using a one-equation closure model. One of their conclusions is that the energy input rate may decrease significantly as the wave slope increases. However, their calculation is rather complicated and involves some empirical parameters. Since our aim is to study the complex effect of wind shear on the nonlinear dynamics of wave instability, the following relatively simple turbulence model will be adopted.

Specifically, in the absence of waves the basic shear flow in air and in water is log–linear with a constant eddy viscosity near the water surface. Wave-induced disturbances, however, are assumed to satisfy the Reynolds equations with constant eddy viscosity. This approach is analogous to the quasi-laminar approximation used by Miles (1957), Valenzuela (1976), Kawai (1979) and others for air flow over

However, in this study we confine ourselves to the most unstable eigenmode as the initial condition of the nonlinear calculations, since many experimental evidences suggest that actually observable instability corresponds to the most unstable mode. The inclusion of the fourth-order (Dysthe's) terms is then necessary to achieve asymmetry or frequency downshift.

gravity–capillary waves, who used a laminar kinematic viscosity near the water surface. Moreover the eddy viscosity in air is proportional to the air friction velocity u'_* and is defined to be

$$\nu'_e = \tilde{\kappa} u'_* \frac{1}{k}, \tag{2.1}$$

where $\tilde{\kappa}$ is an empirical constant and k is the surface wavenumber. Primes are used to designate quantities associated with air. The value of $\tilde{\kappa}$ is later chosen to be 0.02 so that the linear growth rate of surface waves matches Plant's (1982) empirical formula. It will be also shown that our model gives predictions in reasonably close agreement with that of Gent & Taylor (1976) for a finite wave slope based on a more complex turbulence closure model.

In water a constant eddy viscosity,

$$\nu_e = \tilde{\kappa} u_* \frac{1}{k}, \tag{2.2}$$

is introduced similarly, where u_* is the friction velocity in water and $\tilde{\kappa}$ is the same coefficient as in air. Since

$$u_* = \left(\frac{\tau_s}{\rho}\right)^{\frac{1}{2}}, \quad u'_* = \left(\frac{\tau_s}{\rho'}\right)^{\frac{1}{2}} \tag{2.3}$$

where ρ and ρ' are the densities of water and air respectively, and τ_s is the shear stress on the undisturbed interface, ν_e and ν'_e are related by

$$\frac{\nu'_e}{\nu_e} = \left(\frac{\rho}{\rho'}\right)^{\frac{1}{2}} \gg 1. \tag{2.4}$$

In addition to the constant $\tilde{\kappa}$, the surface drift velocity U_d at the horizontal air–water interface is another empirical parameter, which is needed if one assumes that the velocity in water diminishes to zero at great depth in some manner (e.g. exponential). To avoid this additional parameter we follow a Cartesian coordinate system X, Y fixed with the surface drift (directed from left to right) and subtract the wind drift velocity U_d from the total velocity observed by a stationary observer.

In air, we asume the following linear–logarithmic velocity profile:

$$\begin{aligned} U'^s &= \frac{u'^2_*}{\nu'_e} Y \qquad \left(Y < 5\frac{\nu'_e}{u'_*}\right) \\ &= 5u'_* + \frac{u'_*}{\kappa}(\alpha - \tanh\tfrac{1}{2}\alpha) \quad \left(Y > 5\frac{\nu'_e}{u'_*}\right), \end{aligned} \tag{2.5}$$

and

$$\sinh\alpha = 2\kappa \frac{u'_*}{\nu'_e}\left(Y - 5\frac{\nu'_e}{u'_*}\right) \tag{2.6}$$

where Y is the vertical (upward) coordinate measured from the waveless water surface, $\kappa = 0.4$ is the Kármán constant, and $5\nu'_e/u'_*$ can be regarded as the thickness of the sublayer of constant eddy viscosity. The superscript s stands for 'steady' flow without waves. The profile (2.5) has been used by Miles (1957) and Kawai (1979) for air flow over gravity–capillary waves, if the eddy viscosity ν'_e here is replaced by the kinematic viscosity ν'. Inside the sublayer of constant eddy viscosity, the profile is linear. In the limit of $Y \to \infty$, the profile becomes approximately logarithmic.

The induced water current profile is also assumed to be linear–logarithmic:

$$U^{\mathrm{s}} = \frac{u_*^2}{\nu_{\mathrm{e}}} Y \qquad \left(Y > -5\frac{\nu_{\mathrm{e}}}{u_*}\right)$$

$$= -5u_* + \frac{u_*}{\kappa}(\alpha - \tanh\tfrac{1}{2}\alpha) \quad \left(Y < -5\frac{\nu_{\mathrm{e}}}{u_*}\right), \tag{2.7}$$

where

$$\sinh\alpha = 2\kappa\frac{u_*}{\nu_{\mathrm{e}}}\left(Y + 5\frac{\nu_{\mathrm{e}}}{u_*}\right). \tag{2.8}$$

Both profiles are assumed to be established in air and water immediately after the onset of wind.

3. Governing equations for wave-induced disturbances

Let X be the direction of wind and wave propagation, and T denote time. The wave-induced velocities in the X, Y directions and the dynamic pressure are denoted respectively by U, V, P in water and U', V', P' in air. Let us also introduce the following normalization

$$\left.\begin{aligned} (u, v, u', v') = \frac{(U, V, U', V')}{(g/k)^{\frac{1}{2}}}, \quad p = \frac{P}{\rho g/k}, \quad p' = \frac{P'}{\rho' g/k}, \\ x = kX, \quad y = kY, \quad t = (gk)^{\frac{1}{2}} T \end{aligned}\right\} \tag{3.1}$$

where k is the characteristic wavenumber of the free surface, g the acceleration due to gravity, ρ and ρ' densities of water and air respectively. For later calculations the following values chosen for the temperature of 20 °C are used.

$$\rho = 0.998\ \mathrm{g/cm^3}, \quad \rho' = 0.00121\ \mathrm{g/cm^3}, \quad g = 980\ \mathrm{cm/s^2}. \tag{3.2}$$

The normalized governing equations in water for wave induced disturbances are

$$\frac{\partial u}{\partial x} + \frac{\partial v}{\partial y} = 0, \tag{3.3}$$

$$\frac{\partial u}{\partial t} + (u + u^{\mathrm{s}})\frac{\partial u}{\partial x} + v\frac{\partial (u + u^{\mathrm{s}})}{\partial y} = -\frac{\partial p}{\partial x} + \sigma_{\mathrm{e}}^2 \nabla^2 u, \tag{3.4}$$

$$\frac{\partial v}{\partial t} + (u + u^{\mathrm{s}})\frac{\partial v}{\partial x} + v\frac{\partial v}{\partial y} = -\frac{\partial p}{\partial y} + \sigma_{\mathrm{e}}^2 \nabla^2 v, \tag{3.5}$$

$$\nabla^2 = \frac{\partial^2}{\partial x^2} + \frac{\partial^2}{\partial y^2}, \tag{3.6}$$

with the normalized eddy viscosity

$$\sigma_{\mathrm{e}}^2 = \nu_{\mathrm{e}}\left(\frac{k^3}{g}\right)^{\frac{1}{2}}. \tag{3.7}$$

The corresponding equations for wave induced disturbances in air are obtained similarly by adding primes to all dependent variables, u^{s}, ν_{e}, and σ_{e} in (3.3)–(3.7).

They will be referred to as (3.3)′ to (3.7)′ respectively. Introducing the definitions of the eddy viscosities (2.1) and (2.2), the eddy viscosity parameters σ_e^2, and $\sigma_e'^2$ are related to the normalized friction velocity u_*'/C as follows:

$$\sigma_e'^2 = \tilde{\kappa}\frac{u_*'}{C}, \quad \sigma_e^2 = \tilde{\kappa}\frac{u_*}{C} = \tilde{\kappa}\left(\frac{\rho'}{\rho}\right)^{\frac{1}{2}}\frac{u_*'}{C}, \tag{3.8a, b}$$

where $C = (g/k)^{\frac{1}{2}}$ is the phase velocity of surface waves.

Note that the moving coordinates and the corresponding velocity components are related to the absolute stationary coordinates and the velocity components therein by

fixed		translating at u_d
x_0	→	$x = x_0 - u_d t_0$
y_0	→	$y = y_0$
t_0	→	$t = t_0$
u_0	→	$u = u_0 - u_d$
v_0	→	$v = v_0$

In particular the convective derivatives are unchanged,

$$\frac{\partial u_0}{\partial t_0} + u_0\frac{\partial u_0}{\partial x_0} \to \frac{\partial u}{\partial t} + u\frac{\partial u}{\partial x}, \tag{3.9}$$

so that the governing field equations retain the same form for different velocity fields.

On the water surface $y = \zeta(x, t)$, the kinematic boundary conditions are

$$\frac{\partial \zeta}{\partial t} + (u + u^s)\frac{\partial \zeta}{\partial x} - v = \frac{\partial \zeta}{\partial t} + (u' + u'^s)\frac{\partial \zeta}{\partial x} - v' = 0 \quad (y = \zeta), \tag{3.10}$$

$$u + u^s = u' + u'^s, \quad v = v' \quad (y = \zeta). \tag{3.11a, b}$$

As for the dynamic boundary conditions on the water surface we require that the tangential stresses are continuous:

$$\sigma_e^2\left[2\frac{\partial u}{\partial x}n_x n_y + \left(\frac{\partial u}{\partial y} + \frac{\partial v}{\partial x}\right)(n_y n_y - n_x n_x) - 2\frac{\partial v}{\partial y}n_x n_y\right]$$

$$= \frac{\rho'\sigma_e'^2}{\rho}\left[2\frac{\partial u'}{\partial x}n_x n_y + \left(\frac{\partial u'}{\partial y} + \frac{\partial v'}{\partial x}\right)(n_y n_y - n_x n_x) - 2\frac{\partial v'}{\partial y}n_x n_y\right] \quad (y = \zeta), \tag{3.12}$$

as are the normal stresses

$$-p + y + \sigma_e^2\left[2\frac{\partial u}{\partial x}n_x n_x + 2\frac{\partial v}{\partial y}n_y n_y + 2\left(\frac{\partial u}{\partial y} + \frac{\partial v}{\partial x}\right)n_x n_y\right]$$

$$= \frac{\rho'}{\rho}\left\{-p' + y + \sigma_e'^2\left[2\frac{\partial u'}{\partial x}n_x n_x + 2\frac{\partial v'}{\partial y}n_y n_y + 2\left(\frac{\partial u'}{\partial y} + \frac{\partial v'}{\partial x}\right)n_x n_y\right]\right\} \quad (y = \zeta) \tag{3.13}$$

where

$$n_x = \frac{1}{(1 + (\partial\zeta/\partial x)^2)^{\frac{1}{2}}}\left(-\frac{\partial \zeta}{\partial x}\right), \quad n_y = \frac{1}{(1 + (\partial\zeta/\partial x)^2)^{\frac{1}{2}}} \tag{3.14}$$

are the x, y components of a unit vector normal to the wave surface.

Let us now introduce a small parameter ϵ characterizing the wave steepness

$$\epsilon \equiv ka_0, \tag{3.15}$$

where k and a_0 are the wavenumber and the representative wave amplitude respectively. The same parameter also serves as the measure of the timescale and lengthscale of amplitude modulation, i.e. the width of the narrow-banded spectrum of the waves, thus allowing nonlinearity and dispersion to be comparable. We are particularly interested in the circumstances where both the eddy-viscous damping and the wind energy input are comparable and occur over the same timescale as the asymmetric evolution of the Benjamin–Feir instability, which is known to be $t = O(\epsilon^{-3})$ (Lo & Mei 1985). Similar to the case of molecular viscosity the normalized damping rate is of $O(\sigma_e^2)$, hence we set

$$\sigma_e^2 \equiv N\epsilon^3 \tag{3.16}$$

where N is a constant of $O(1)$.

In terms of the normalized variables the basic wind profile is

$$\begin{aligned} u'^s &= s'y && (y < 5\tilde{\kappa}) \\ &= s'\left[5\tilde{\kappa} + \frac{\tilde{\kappa}}{\kappa}(\alpha - \tanh\tfrac{1}{2}\alpha)\right] && (y > 5\tilde{\kappa}), \end{aligned} \tag{3.17}$$

where

$$\sinh\alpha = 2\frac{\kappa}{\tilde{\kappa}}(y - 5\tilde{\kappa}), \tag{3.18}$$

and the normalized wind shear s' is

$$s' = \frac{u_*'^2}{\nu_e'(gk)^{\frac{1}{2}}} = \frac{u_*'^2}{\tilde{\kappa}(u_*'/k)(gk)^{\frac{1}{2}}} = \frac{1}{\tilde{\kappa}}\frac{u_*'}{C}. \tag{3.19}$$

Similarly the normalized water current profile is

$$\begin{aligned} u^s &= sy && (y > -5\tilde{\kappa}) \\ &= s\left[-5\tilde{\kappa} + \frac{\tilde{\kappa}}{\kappa}(\alpha - \tanh\tfrac{1}{2}\alpha)\right] && (y < -5\tilde{\kappa}), \end{aligned} \tag{3.20}$$

where

$$s = \frac{1}{\tilde{\kappa}}\frac{u_*}{C} = \left(\frac{\rho'}{\rho}\right)^{\frac{1}{2}} s', \quad \sinh\alpha = 2\frac{\kappa}{\tilde{\kappa}}(y + 5\tilde{\kappa}). \tag{3.21}$$

By eliminating p and p' the normal stress boundary condition (3.13) may be written in terms of velocity components. Using the fact that $\rho'/\rho \ll 1$ we shall keep the most important terms on the right-hand side to get

$$\begin{aligned} &\left(\frac{\partial u}{\partial t} + (u+u^s)\frac{\partial u}{\partial x} + v\frac{\partial(u+u^s)}{\partial y} - \sigma_e^2\nabla^2 u\right) + \left(\frac{\partial v}{\partial t} + (u+u^s)\frac{\partial v}{\partial x} + v\frac{\partial v}{\partial y} - \sigma_e^2\nabla^2 v\right)\frac{\partial \zeta}{\partial x} \\ &\quad + \frac{\partial \zeta}{\partial x} + \sigma_e^2\left(\frac{\partial}{\partial x} + \frac{\partial \zeta}{\partial x}\frac{\partial}{\partial y}\right)\left[2\frac{\partial u}{\partial x}n_x n_x + 2\frac{\partial v}{\partial y}n_y n_y + 2\left(\frac{\partial u}{\partial y} + \frac{\partial v}{\partial x}\right)n_x n_y\right] \\ &\quad = -\frac{\rho'\sigma_e'^2}{\rho}\frac{\partial^2 u'}{\partial y^2}[1 + O(\epsilon, \delta'^2)] \equiv \frac{\partial f_b'}{\partial x} \quad (y = \zeta), \end{aligned} \tag{3.22}$$

where f_b' is the non-dimensional normal stress due to wind, and $\delta' \ll 1$ is the

normalized boundary-layer thickness in air whose order of magnitude will be examined in §4. Details are given in Appendix A. Similarly the tangential stress boundary condition (3.12) can be approximated by

$$\sigma_e^2\left[2\frac{\partial u}{\partial x}n_x n_y+\left(\frac{\partial u}{\partial y}+\frac{\partial v}{\partial x}\right)(n_y n_y-n_x n_x)-2\frac{\partial v}{\partial y}n_x n_y\right]$$

$$=\frac{\rho'\sigma_e'^2}{\rho}\frac{\partial u'}{\partial y}[1+O(\epsilon,\delta'^2)]\equiv f_a' \quad (y=\zeta), \tag{3.23}$$

where f_a' is the non-dimensional tangential stress. The ratio of the tangential stress (3.23) to the normal stress (3.22) is

$$\frac{f_a'}{f_b'}\sim\frac{(\rho'\sigma_e'^2/\rho)(\partial u'/\partial y)}{(\rho'\sigma_e'^2/\rho)(\partial^2 u'/\partial y^2)}=O(\delta')\ll 1. \tag{3.24}$$

It will be shown later that the normal stress is more important than the tangential stress in transferring energy from wind to waves. However, the tangential stress component affects the phase and group velocities of water waves by modifying the mean shear current in water, as will be shown in §6.

We now return to the basic assumption that the growth of the waves due to wind occurs in the timescale of $O(\epsilon^3)$. Recall that the dimensionless wave amplitude is of $O(\epsilon)$, and the wave energy is of $O(\epsilon^2)$. Since the assumed timescale for energy variation is $O(\epsilon^3)$, the implied rates of energy input and attenuation must be of $O(\epsilon^5)$. The major source of forcing for wave growth is the product of the normal stress (3.22) and the vertical velocity of $O(\epsilon)$ at the surface. It follows that the magnitude of the normal stress must be of $O(\epsilon^4)$. Therefore, we shall later choose the wind strength so that the right-hand side of (3.22) becomes of $O(\epsilon^4)$. In nature the wind strength can be quite arbitrary, but the more general situation cannot be conveniently treated here.

4. Air flow over gravity waves

In this section and the next our objective is to solve the air flow over gravity waves, and calculate the surface stresses imposed on waves due to wind. Since the effect of wind appears at the highest order in the evolution of wave amplitude (fourth-order in wave steepness), it is sufficient to obtain the air flow within the accuracy (i.e. error) of $O(\epsilon)$. First, the kinematic boundary conditions for air at the interface need to be specified, which depends on the leading-order wave motion in water. Although the wind strength is not yet specified, we estimate tentatively that the wind-induced current in water is weak ($u^s\sim s=O(\epsilon)$) so that the leading-order wave motion is not affected by the current. The validity of this estimation must be confirmed when we give the specific magnitude of wind strength later. Since for water waves the effect of air is negligible up to $O(\epsilon^4)$, the linearized results can be used to calculate air motion

$$\zeta=\tfrac{1}{2}\epsilon A\,e^{i(x-t)}+*, \tag{4.1}$$

$$u=\epsilon\tfrac{1}{2}A\,e^{y}e^{i(x-t)}+*, \quad v=-\epsilon\tfrac{1}{2}Ai\,e^{y}e^{i(x-t)}+*, \tag{4.2a, b}$$

where A is the complex wave amplitude of $O(1)$ and can be a function of slow variables in x and t. The dimensional wave amplitude a is related to A by

$$\epsilon|A|=ka. \tag{4.3}$$

For the analysis of the air flow we set

$$A = B\mathrm{e}^{\mathrm{i}D}, \tag{4.4}$$

where B and D are the absolute amplitude and the phase of the complex wave amplitude A. We then introduce a new coordinate

$$x' = x - t + D, \tag{4.5}$$

which follows the phase velocity of the wave. The velocities u'^{s}, u' remain unchanged, i.e. they are still measured in the frame of reference fixed to the surface drift. Then the kinematic boundary conditions for air motion at the interface are inferred from the wave solution (4.1)–(4.2) as

$$u' + u'^{\mathrm{s}} = u + u^{\mathrm{s}} = \epsilon B \cos x' \quad (y = \zeta), \tag{4.6}$$

$$v' = v = \epsilon B \sin x' \quad (y = \zeta), \tag{4.7}$$

$$\zeta = \epsilon B \cos x', \tag{4.8}$$

to the leading order. With this new coordinate, the boundary conditions for air are independent of the short timescale t. Thus the air flow can be treated as steady in the timescale of $t = O(1)$. Let us introduce a stream function $\psi' + \psi'^{\mathrm{s}}$ where

$$\frac{\partial \psi'^{\mathrm{s}}}{\partial y} = u'^{\mathrm{s}} \tag{4.9}$$

is the basic turbulent air flow given in (3.17), and

$$\frac{\partial \psi'}{\partial y} = u', \quad -\frac{\partial \psi'}{\partial x'} = v', \tag{4.10}$$

are the disturbances due to waves.

It is now convenient to introduce the following orthogonal curvilinear coordinates ξ', η defined by

$$x' = \xi' - \epsilon B \sin \xi' \, \mathrm{e}^{-\eta}, \tag{4.11}$$

$$y = \eta + \epsilon B \cos \xi' \, \mathrm{e}^{-\eta}, \tag{4.12}$$

which are known to map the Stokes wave profile onto a flat surface up to $O(\epsilon)$. Therefore, they are accurate enough in order to solve the air flow to the leading order in ϵ. The governing equation in the mapped plane for the wave perturbation ψ' may be derived by eliminating p' from (3.4)′ and (3.5)′ as

$$-\frac{\partial[\psi'^{\mathrm{s}} - y, (1/J)\nabla'^2\psi']}{\partial(\xi', \eta)} - \frac{\partial[\psi', (\partial^2\psi'^{\mathrm{s}}/\partial y^2)]}{\partial(\xi', \eta)} - \frac{\partial[\psi', (1/J)\nabla'^2\psi']}{\partial(\xi', \eta)}$$

$$= \sigma_{\mathrm{e}}'^2 \nabla'^2[(1/J)\nabla'^2\psi'], \tag{4.13}$$

$$\nabla'^2 \equiv \frac{\partial}{\partial \xi'^2} + \frac{\partial}{\partial \eta^2}, \tag{4.14}$$

where J is the Jacobian of transformation and can be approximated by 1 to the leading order. In the first term the negative current $-y$ is added because of the shift of coordinates according to (4.5).

The surface boundary conditions are inferred from (4.6) and (4.7) as

$$\frac{\partial \psi'}{\partial \xi'} = -\frac{\partial \psi'^{\mathrm{s}}}{\partial \xi'} - \epsilon B \sin \xi' \quad (\eta = 0), \tag{4.15}$$

$$\frac{\partial \psi'}{\partial \eta} = -\frac{\partial \psi'^{\mathrm{s}}}{\partial \eta} + \epsilon B \cos \xi' \quad (\eta = 0). \tag{4.16}$$

In particular if the waves are immersed inside the sublayer of constant eddy viscosity ($\epsilon B < 5\tilde{\kappa}$), the boundary conditions are simplified as

$$\begin{aligned} \frac{\partial \psi'}{\partial \xi'} &= -\left(\frac{\partial \psi'^{\mathrm{s}}}{\partial y}\frac{\partial y}{\partial \xi'}\right)_{\eta=0} - \epsilon B \sin \xi' \\ &= -s'[(\eta + \epsilon B \cos \xi' \, \mathrm{e}^{-\eta})(-\epsilon B \sin \xi' \, \mathrm{e}^{-\eta})]_{\eta=0} - \epsilon B \sin \xi' \\ &= \tfrac{1}{2} s' (\epsilon B)^2 \sin 2\xi' - \epsilon B \sin \xi' \quad (\eta = 0). \end{aligned} \tag{4.17}$$

Similarly

$$\begin{aligned} \frac{\partial \psi'}{\partial \eta} &= -\left(\frac{\partial \psi'^{\mathrm{s}}}{\partial y}\frac{\partial y}{\partial \eta}\right)_{\eta=0} + \epsilon B \cos \xi' \\ &\approx -s' \epsilon B \cos \xi' + \epsilon B \cos \xi' \quad (\eta = 0). \end{aligned} \tag{4.18}$$

At infinity we allow a finite increase/decrease of wind speed, and impose

$$\frac{\partial \psi'}{\partial \eta} = \text{const}, \quad \frac{\partial \psi'}{\partial \xi'} = 0 \quad (\eta = \infty). \tag{4.19a, b}$$

Note that by definition $B = O(1)$. The magnitude of the wind shear s' is not yet specified. We now show that the nonlinear term in (4.13) is not necessarily small inside the air boundary layer. The dominant term on the left-hand side of (4.13) is

$$\frac{\partial(\psi'^{\mathrm{s}} - y)}{\partial \eta} \frac{\partial^3 \psi'}{\partial \eta^2 \partial \xi'}, \tag{4.20}$$

which should be balanced by the dominant dissipation term

$$\sigma'^2_{\mathrm{e}} \frac{\partial^4 \psi'}{\partial \eta^4}, \tag{4.21}$$

on the right-hand side. Let us define the air boundary-layer thickness to be δ'. Referring to (3.17) the basic wind velocity near the interface is

$$\frac{\partial \psi'^{\mathrm{s}}}{\partial \eta} \sim s' \delta', \tag{4.22}$$

and the added steady current (the negative of the phase velocity) is

$$-\frac{\partial y}{\partial \eta} \sim -1. \tag{4.23}$$

For relatively weak wind ($s'\delta' \leqslant O(1)$) the boundary-layer thickness δ' is estimated by balancing (4.20) and (4.21) with (4.23), i.e.

$$\delta' \sim \sigma'_{\mathrm{e}} \quad \text{if } s'\delta' \sim s'\sigma'_{\mathrm{e}} \leqslant O(1). \tag{4.24}$$

For relatively strong wind ($s'\delta' \geqslant O(1)$) the balance of (4.20) and (4.21) with (4.22) gives

$$\delta' \sim \left(\frac{\sigma_e'^2}{s'}\right)^{\frac{1}{3}} \leqslant \sigma_e' \quad \text{if } s'\delta' \sim (s'\sigma_e')^{\frac{2}{3}} \geqslant O(1) \quad (\text{or } s'\sigma_e' \geqslant O(1)). \tag{4.25}$$

Therefore the boundary-layer thickness δ' is at most of $O(\sigma_e')$.

In the boundary condition (4.16) or (4.18) the magnitude of $\partial\psi'/\partial\eta$ is of $O(\epsilon s')$. Thus the magnitude of the perturbed convective inertia relative to the linearized convective inertia is approximately

$$\left.\frac{\partial\psi'}{\partial\eta}\frac{\partial^3\psi'}{\partial\eta^2\partial\xi'}\right/\frac{\partial(\psi'^s-y)}{\partial\eta}\frac{\partial^3\psi'}{\partial\eta^2\partial\xi'} \sim \epsilon s' \quad \text{if } \sigma_e' s' \leqslant O(1)$$

$$\sim \frac{\epsilon}{\delta'} \quad \text{if } \sigma_e' s' \geqslant O(1). \tag{4.26}$$

In the next section, the range of s' to be chosen in our calculations is somewhat larger than 1, and δ' is always much smaller than $O(1)$. Thus in both cases the ratio (4.26) is not neglible, and all the nonlinear terms in (4.13) must be kept. This observation suggests that the energy input rate from air to water through surface stresses depends on the wave steepness ka to the leading order, unlike Janssen's (1986) model in which the wave growth rate is assumed to be constant.

Referring to the governing equation (4.13) and boundary conditions (4.15), (4.16), (4.19) for ψ' as well as the basic shear profile (3.17), the air-flow problem is controlled by three parameters; the shear rate s' in air, the wave slope $\epsilon B = ka$, and the eddy viscosity parameter $\sigma_e'^2$. Since both $\sigma_e'^2$ and s' are related to the normalized friction velocity u_*'/C through (3.8a) and (3.19), the air flow depends only on two non-dimensional parameters u_*'/C and ϵB.

5. Numerical solution for the air flow

5.1. *Method of solution*

Since the governing equation and boundary conditions for the perturbation stream function ψ' are nonlinear but steady, we can employ the spectral method used before by Caponi *et al.* (1982), who solved a similar mathematical problem with a constant laminar viscosity. On introducing the Fourier expansion,

$$\psi' = \epsilon B \sum_n f_n(\eta)\, e^{in\xi'}, \tag{5.1}$$

into (4.13), we obtain an infinite set of coupled nonlinear ordinary differential equations for $f_n(\eta)$. In the actual calculation this series is truncated at $n = \pm n_M$, and the coupled equations are approximated by finite differences with exponentially increasing separation between adjacent grid points:

$$\eta_0 = 0, \eta_1, \eta_2, \ldots, \eta_M = \eta_{\max},$$

$$\frac{\eta_{n+1}-\eta_n}{\eta_n-\eta_{n-1}} = r = \text{const} > 1. \tag{5.2}$$

The boundary conditions at $\eta = \infty$ are applied at $\eta = \eta_{\max}$ instead. The resulting nonlinear coupled algebraic equations are solved by Newton–Ralphson iteration.

After trial and error the following values are found to be satisfactory in the calculations.

$$n_M = 6, \quad M = 200, \quad \eta_{\max} = 7.0, \quad r = 1.024 \tag{5.3}$$

5.2. *Surface stresses and energy transfer at the interface*

The calculated result of ψ' is now introduced to the right-hand side of (3.22) in order to calculate the x-derivative of the normal stress within the accuracy of $O(\epsilon, \delta'^2)$:

$$\frac{\partial f'_{\mathrm{b}}}{\partial x} \approx -\frac{\rho'\sigma'^2_{\mathrm{e}}}{\rho}\left(\frac{\partial^2 u'}{\partial y^2}\right)_{y=\zeta} \approx -\frac{\rho'\sigma'^2_{\mathrm{e}}\,\epsilon B}{\rho}\sum_n \left(\frac{\partial^3 f_n}{\partial \eta^3}\right)_{\eta=0} \mathrm{e}^{\mathrm{i}n(x-t)}\,\mathrm{e}^{\mathrm{i}nD}. \tag{5.4}$$

So far the numerical program is valid for any s'. We now choose the wind strength s' so that the magnitude of (5.4) becomes of $O(\epsilon^4)$ as has been discussed before. For later convenience we formally represent the normal stress forcing by

$$\frac{\partial f'_{\mathrm{b}}}{\partial x} = N\epsilon^4 \sum_n p_n \mathrm{e}^{\mathrm{i}n(x-t)}. \tag{5.5}$$

Of particular significance is the coefficient of the first harmonic,

$$p_1 = -\frac{1}{N\epsilon^4}\frac{\rho'\sigma'^2_{\mathrm{e}}\,\epsilon B}{\rho}\left(\frac{\partial^3 f_1}{\partial \eta^3}\right)_{\eta=0}\frac{A}{B} = -A\left(\frac{\rho'}{\rho}\right)^{\frac{1}{2}}\left(\frac{\partial^3 f_1}{\partial \eta^3}\right)_{\eta=0} = O(1), \tag{5.6}$$

which is responsible for the growth and the phase shift of surface waves. Similarly the right-hand side of the tangential stress boundary condition (3.23) can be calculated as

$$f'_{\mathrm{a}} \approx \frac{\rho'\sigma'^2_{\mathrm{e}}}{\rho}\left(\frac{\partial u'}{\partial y}\right)_{y=\zeta} \approx \frac{\rho'\sigma'^2_{\mathrm{e}}\,\epsilon B}{\rho}\sum_n \left(\frac{\partial^2 f_n}{\partial \eta^2}\right)_{\eta=0} \mathrm{e}^{\mathrm{i}n(x-t)}\,\mathrm{e}^{\mathrm{i}nD}. \tag{5.7}$$

Although f'_{a} is smaller than the normal stress (5.4) by a factor of δ', as has been discussed in (3.24), we may also set formally

$$f'_{\mathrm{a}} = N\epsilon^4 \sum_n q_n \mathrm{e}^{\mathrm{i}n(x-t)}. \tag{5.8}$$

Note that the magnitude of the first harmonic q_1 is of $O(\delta') \ll 1$.

The zeroth harmonic f_0 of ψ' arises as a result of nonlinearity in the governing equation (4.13). Therefore the magnitude of f_0 compared to that of f_1 (or q_0/q_1) is approximately

$$\begin{aligned} \frac{f_0}{f_1} \sim \frac{q_0}{q_1} &\sim \epsilon s' \quad \text{if } \sigma'_{\mathrm{e}} s' \leqslant O(1) \\ &\sim \frac{\epsilon}{\delta'} \quad \text{if } \sigma'_{\mathrm{e}} s' \geqslant O(1), \end{aligned} \tag{5.9}$$

based on the analysis in §4. Hence

$$\begin{aligned} q_0 \sim q_1\left(\frac{q_0}{q_1}\right) \sim \epsilon s'\delta' \sim \epsilon s'\sigma'_{\mathrm{e}} \leqslant O(\epsilon) \quad &\text{if } \sigma'_{\mathrm{e}} s' \leqslant O(1) \\ \sim \epsilon \qquad\qquad\qquad\qquad\quad &\text{if } \sigma'_{\mathrm{e}} s' \geqslant O(1), \end{aligned} \tag{5.10}$$

and in both cases q_0 is of $O(\epsilon)$ or smaller. The zeroth harmonic q_0 is the spatially averaged shear stress due to the presence of waves, and may be considered as a

correction to the basic shear s. The effect of q_0 on the evolution equation of surface wave amplitude appears through modified water current ψ_{20} and will be thoroughly discussed in §6.

Let us calculate the energy input rate W from air to water through the normal stress. From (5.5), the first harmonic of the normal stress f'_b is given as

$$N\epsilon^4 \frac{p_1}{i} e^{i(x-t)} + *. \tag{5.11}$$

By multiplying this first harmonic and the vertical orbital velocity v (4.2b), and taking the time average, we obtain the energy input rate

$$W = \overline{\left[N\epsilon^4 \frac{p_1}{i} e^{i(x-t)} + *\right][-\epsilon \tfrac{1}{2} A i e^{i(x-t)} + *]} = N\epsilon^5 |A|^2 \operatorname{Re}\left(\frac{p_1}{A}\right), \tag{5.12}$$

where the overbar indicates the time average and Re ( ) the real part of ( ). The energy input rate through the tangential stress f'_a is smaller than that of f'_b by $O(\delta')$ and is neglected. Since the normalized wave energy E per unit length is

$$E = \tfrac{1}{2}\epsilon^2 |A|^2, \tag{5.13}$$

the normalized energy input rate $\tilde{\beta}^r$ from wind to waves is

$$\tilde{\beta}^r = \frac{W}{E} = 2N\epsilon^3 \operatorname{Re}\left(\frac{p_1}{A}\right) = 2\sigma_e^2 \operatorname{Re}\left(\frac{p_1}{A}\right). \tag{5.14}$$

The corresponding imaginary part of p_1/A is also defined as

$$\tilde{\beta}^i = 2\sigma_e^2 \operatorname{Im}\left(\frac{p_1}{A}\right), \tag{5.15}$$

which is responsible for the phase shift of surface waves.

The turbulent dissipation rate $\tilde{\beta}^d$ due to the constant eddy viscosity ν_e in water is

$$\tilde{\beta}^d = 4\sigma_e^2 \tag{5.16}$$

by analogy to the laminar viscous dissipation rate. Hence the net growth rate is

$$\tilde{\beta} = \tilde{\beta}^r - \tilde{\beta}^d = \sigma_e^2 \left[2 \operatorname{Re}\left(\frac{p_1}{A}\right) - 4\right]. \tag{5.17}$$

In particular the initial linear growth rate is

$$\tilde{\beta}_0 = \tilde{\beta}_0^r - \tilde{\beta}^d = \tilde{\beta}^r|_{|A|=0} - \tilde{\beta}^d = \sigma_e^2 \left[2 \operatorname{Re}\left(\frac{p_1}{A}\right)_{|A|=0} - 4\right] + O(\epsilon, \delta'). \tag{5.18}$$

As pointed out at the end of §4, the air flow is controlled by two parameters u'_*/C and $\epsilon B = ka$. Therefore the coefficient

$$\frac{p_1}{A} = \left(\frac{\rho'}{\rho}\right)^{\frac{1}{2}} \left(-\frac{\partial^3 f_1}{\partial \eta^3}\right)_{\eta=0}, \tag{5.19}$$

depends on these two parameters. Since σ_e^2 is related to u'_*/C by (3.8b), the growth rate $\tilde{\beta}$ is also a function of u'_*/C and $\epsilon B = ka$. In the limit of $|A| = B = 0$ the linear growth rate $\tilde{\beta}_0$ is a function of u'_*/C only.

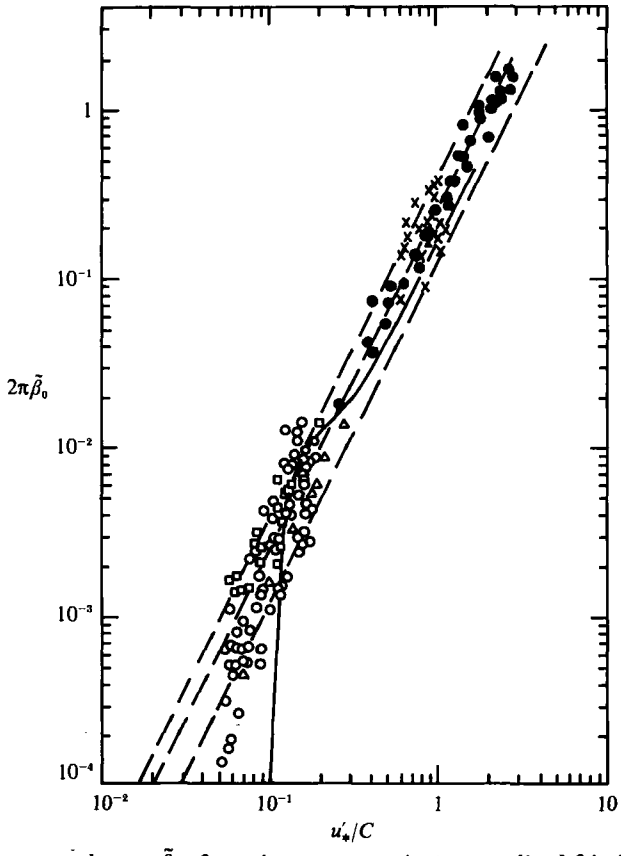

FIGURE 1. Linear growth rate $\tilde{\beta}_0$ of gravity waves against normalized friction velocity u'_*/C. Solid line, our result; ---, Plant (1982); △, Shemdin & Hsu (1967); ●, Larson & Wright (1975); ×, Wu *et al.* (1977, 1979); ○, Snyder *et al.* (1981), fixed sensors; □, Snyder *et al.* (1981), wave-following sensor.

Based on many laboratory and field experiments Plant (1982) has given an empirical linear growth rate of gravity waves,

$$\tilde{\beta}_0 = (0.04 \pm 0.02)\left(\frac{u'_*}{C}\right)^2, \tag{5.20}$$

for $k > 0.63$ cm^{-1} and $u'_*/C > 0.07$. Mitsuyasu & Honda (1982) have later shown that this empirical growth rate is valid up to $k > 0.024$ cm^{-1}. We have found that if

$$\tilde{\kappa} = 0.02 \tag{5.21}$$

is chosen in the definition of the eddy viscosity (2.1), the numerical results of (5.18) fit the empirical curve (5.20) reasonably well for $u'_*/C > 0.1$ as is shown in figure 1. According to our result the growth rate deviates from (5.20) at $u'_*/C \approx 0.1$ and drops quickly, whereas the experimental results start to deviate around a lower $u'_*/C \approx 0.07$. This discrepancy can in principle be removed by choosing a more complex turbulence model, but this is not pursued here.

With $\tilde{\kappa}$ chosen, the result of the initial growth rate shows that the energy input from wind and the dissipation due to the eddy viscosity are comparable if $u'_*/C = O(0.1)$. We therefore choose three values ($u'_*/C = 0.12, 0.14, 0.16$) of the normalized friction velocity in the later analysis of the long-time evolution of sideband instability.

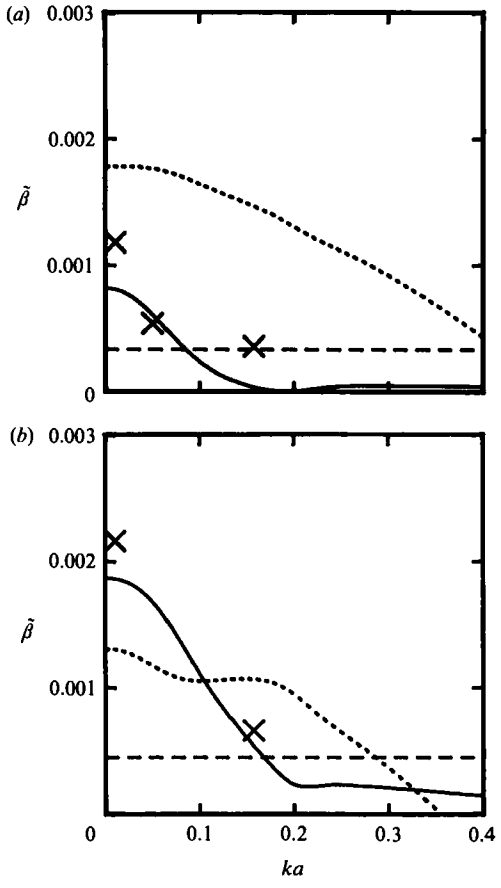

FIGURE 2. ——, Nonlinear energy input rate $\tilde{\beta}^{\mathrm{r}}$; – – –, imaginary part of wind forcing $\tilde{\beta}^{\mathrm{i}}$; — — —, dissipation rate $\tilde{\beta}^{\mathrm{d}}$ as functions of wave slope ka. (*a*) $u'_*/C = 0.12$. ×, Gent & Taylor (1976), $u'_*/C = 0.125$. (*b*) $u'_*/C = 0.16$. ×, Gent & Taylor (1976), $u'_*/C = 0.167$.

In figure 2 the nonlinear growth rate $\tilde{\beta}^{\mathrm{r}}$, the imaginary part of the wind forcing $\tilde{\beta}^{\mathrm{i}}$, and the dissipation rate $\tilde{\beta}^{\mathrm{d}}$ are plotted for $u'_*/C = 0.12, 0.16$, and for a wide range of wave slope $ka = 0$–0.40 including cases which exceed the limits of our theory, in order to speculate the trend of strong nonlinear effects. In all cases the growth rate decreases significantly as the wave steepness increases. This is consistent with the fact that nonlinearity in the governing equation for air is important to the leading order. In particular there exists a equilibrium wave slope $(ka)_{\mathrm{eq}}$ which is still rather small, at which the wind energy input and the dissipation due to turbulence in water cancel out.

Gent & Taylor (1976) calculated the nonlinear energy transfer rate from air to water through surface pressure, by using one-equation closure turbulence model. At first they assumed a constant roughness along the wavy surface, and the result underestimates the linear energy input rate; the nonlinear input rate depends on the wave steepness very weakly. They next assumed that the roughness varies along the surface, simulating the distribution of ripples over gravity waves, and obtained more reasonable initial energy transfer rate. With the second model the nonlinear transfer rate decreases significantly as the wave steepness increases. Clearly the second model is more heuristic than theoretical. Nevertheless, we compare Gent & Taylor's second

u'_*/C	s'	s	σ_e^2	$\sigma_e'^2$
0.10	5	0.18	7.0×10^{-5}	2.0×10^{-3}
0.20	10	0.35	1.4×10^{-4}	4.0×10^{-3}
0.40	20	0.70	2.8×10^{-4}	8.0×10^{-3}

TABLE 1. Typical values of wind shear and viscosity parameters

results with ours in figure 2. The good qualitative agreement of both theories suggests that our simple turbulence model, with only one parameter $\tilde{\kappa}$, is as good as a more involved model in predicting the nonlinear energy transfer rate.

We comment in passing that Jacobs (1987) solved analytically the linear energy transfer rate through surface pressure by assuming that the eddy viscosity is proportional to the vertical distance from the wave surface. His model can in principle be extended for a finite wave amplitude. However with his model the surface roughness has to be given empirically. Also he speculates that the distribution of the eddy viscosity may not be well described by his simple model for finite wave steepness. Therefore we will not examine the possibility of applying his turbulence model to this study.

With the value of $\tilde{\kappa}$ determined as (5.21), we calculate from (3.8) the eddy viscosity parameters σ_e^2, $\sigma_e'^2$, and the normalized shear s' (in air) and s (in water) for typical values of normalized friction velocity u'_*/C. The results are shown in table 1.

At the beginning of §4 we have assumed that the wind-induced current in water is weak:

$$u^s \sim s = O(\epsilon). \tag{5.22}$$

Although the values of s in table 1 for $u'_*/C = 0.12$–0.16 are somewhat larger than $O(\epsilon)$ as estimated, we shall find that the effect of the water shear on the evolution equation (namely coefficients κ_{30}, κ_{60}) are multiplied by a small numerical factor. Therefore the estimation (5.22) is regarded as satisfactory in this study. Introducing the values of table 1 into (4.24) and (4.25), the boundary-layer thickness δ' is estimated to be always less than $O(0.1)$. Therefore it is consistent to neglect terms of $O(\delta')$ as well as those of $O(\epsilon)$.

5.3. *Air flow above the waves and effective roughness height*

We now discuss the computed air flow over surface waves. In figure 3 we plot the stream function contour of $\psi' + \psi'^s - y$ for $u'_*/C = 0.1$, 0.2 and $ka = 0.1$ in the coordinates moving with the phase velocity of the waves. Recall that the velocity field of ψ' is not small compared with that of ψ'^s inside the air boundary layer. In all cases a circulation of air appears at the height where the wind speed in the fixed coordinates is equal to the phase velocity. The location of the circulation migrates from the crest to the trough as the wind speed increases.

Note that in (4.19) the first-derivative of the perturbed air $\partial\psi'/\partial\eta$ is allowed to be finite at $\eta = \infty$. This corresponds to a finite wind velocity shift caused by waves. In the theory of fully turbulent shear flow over a rough plane bed, the velocity profile is known to be

$$\frac{U'}{u'_*} = \frac{1}{\kappa}\ln\frac{Y}{k_s} + 8.5 \tag{5.23}$$

(Schlichting 1955), where k_s is the equivalent surface roughness. For fixed u'_*, as the roughness k_s increases the velocity decreases. If the waves are regarded as a surface

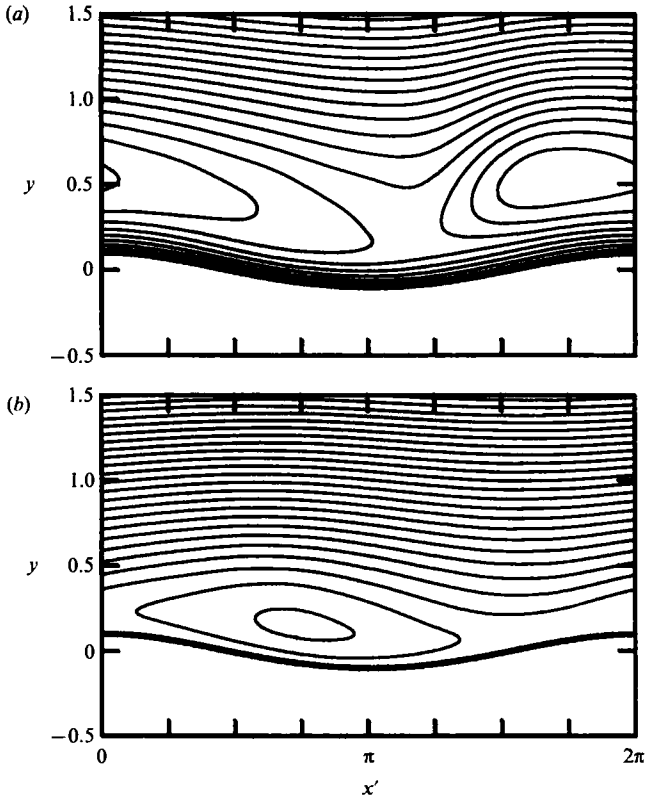

FIGURE 3. Contours of the air flow $\psi' + \psi'^{s} - y$ over surface waves. $ka = 0.1$. Vertical scale is stretched by a factor of 2. (*a*) $u'_*/C = 0.1$, $\Delta\psi' = 0.02$. (*b*) $u'_*/C = 0.2$, $\Delta\psi' = 0.06$.

roughness, the corresponding equivalent roughness k_s must be larger than that of the flat surface without gravity waves (k_{s0}), and the resulting velocity defect is related to the finite $(\partial\psi'/\partial\eta)_{\eta=-\infty}$ as

$$-\frac{u'_*}{C}\frac{1}{\kappa}\ln\frac{k_s}{k_{s0}} = u'|_{y=-\infty} = \left(\frac{\partial\psi'}{\partial\eta}\right)_{\eta=-\infty}. \tag{5.24}$$

From this relationship we can calculate the ratio k_s/k_{s0} against the wave slope ka for various values of wind strength u'_*/C, as shown in figure 4.

When wind is weak ($u'_*/C \leqslant 0.1$), gravity waves have little effect on the equivalent roughness. As the friction velocity increases, the roughness is magnified by waves. This effect becomes most prominent around $u'_*/C = 0.16$–0.20 where the roughness is magnified seven times for $ka = 0.20$. For still stronger wind, our theory, while incomplete, suggests that the roughness is less affected by the presence of gravity waves. The absolute value of the equivalent roughness k_{s0} without gravity waves cannot be easily obtained since different empirical formulae (for example Charnock 1955; Stewart 1974; Jacobs 1987) give vastly different values. Therefore our calculated results can only be used to infer that, for given u'_*, the roughness k_s is the greatest when the phase velocity of the gravity waves is $C \approx 5u'_*$–$6u'_*$ for a fixed wave slope. With shorter or longer waves, k_s decreases. Recently, Plant (1990) has shown from laboratory and field data that for a given u'_* of 0.3–0.8 m/s, the roughness k_s is maximum in a lake (with a fetch of 1–6 km) and is smaller in the ocean (with a fetch of O(100 km)) or in the wave tank of O(10 m). This is qualitatively

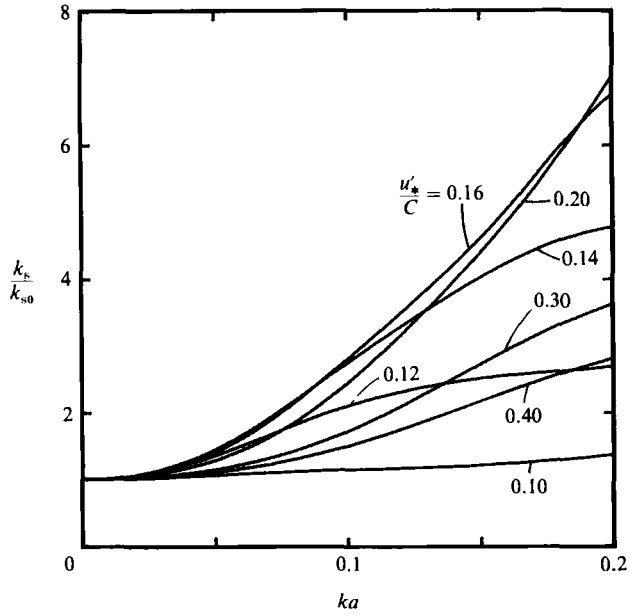

FIGURE 4. The ratio of equivalent roughness k_s over gravity waves to that on a flat surface k_{s0} as a function of wave slope ka for different values of normalized friction velocity u'_*/C.

consistent with figure 4. In particular for $u'_* = 0.8$ m/s the surface roughness becomes maximum around the phase speed of $C = 4$–5 m/s according to figure 4, the corresponding wavelength is 10–16 m, which is the typical wavelength in a lake.

6. Wave motion in water

6.1. *Boundary-layer correction*

In this section we will examine the wave motion in water up to $O(\epsilon^4)$ in order to obtain the long-time evolution equation of wave amplitude A. The motion associated with waves is simply governed by the vorticity equation with a constant eddy viscosity. By eliminating the pressure p from (3.4) and (3.5), the governing equation is obtained as

$$\nabla^2\frac{\partial\psi_T}{\partial t}-\epsilon\frac{\partial(\psi_T,\nabla^2\psi^s)}{\partial(x,y)}-\epsilon\frac{\partial(\psi^s,\nabla^2\psi_T)}{\partial(x,y)}-\epsilon\frac{\partial(\psi_T,\nabla^2\psi_T)}{\partial(x,y)}=N\epsilon^3\nabla^2\nabla^2\psi_T, \tag{6.1}$$

where $\psi_T = O(1)$ is the wave-induced disturbances defined by

$$u=\epsilon\frac{\partial\psi_T}{\partial y},\quad v=-\epsilon\frac{\partial\psi_T}{\partial x}; \tag{6.2}$$

and

$$u^s=\epsilon\frac{\partial\psi^s}{\partial y} \tag{6.3}$$

is the basic water current of $O(\epsilon)$ given by (3.20). The kinematic boundary condition at the surface (3.10) is

$$\frac{\partial\tilde{\xi}}{\partial t}+\epsilon\frac{\partial(\psi_T+\psi^s)}{\partial y}\frac{\partial\tilde{\xi}}{\partial x}+\frac{\partial\psi_T}{\partial x}=0\quad(y=\epsilon\tilde{\xi}), \tag{6.4}$$

where
$$\zeta = \epsilon\tilde{\zeta} \tag{6.5}$$
is the wave surface. The normal stress condition (3.22) with (5.5) reads

$$\begin{aligned}
&\frac{\partial^2\psi_{\mathrm{T}}}{\partial y\,\partial t}+\epsilon\frac{\partial(\psi_{\mathrm{T}}+\psi^{\mathrm{S}})}{\partial y}\frac{\partial^2\psi_{\mathrm{T}}}{\partial y\,\partial x}-\epsilon\frac{\partial\psi_{\mathrm{T}}}{\partial x}\frac{\partial^2(\psi_{\mathrm{T}}+\psi^{\mathrm{S}})}{\partial y^2}-N\epsilon^3\nabla^2\frac{\partial\psi_{\mathrm{T}}}{\partial y}\\
&\quad+\epsilon\left(-\frac{\partial^2\psi_{\mathrm{T}}}{\partial x\,\partial t}-\epsilon\frac{\partial(\psi_{\mathrm{T}}+\psi^{\mathrm{S}})}{\partial y}\frac{\partial^2\psi_{\mathrm{T}}}{\partial x^2}+\epsilon\frac{\partial\psi_{\mathrm{T}}}{\partial x}\frac{\partial^2\psi_{\mathrm{T}}}{\partial x\,\partial y}+N\epsilon^3\nabla^2\frac{\partial\psi_{\mathrm{T}}}{\partial x}\right)\frac{\partial\tilde{\xi}}{\partial x}\\
&\quad+\frac{\partial\tilde{\xi}}{\partial x}+N\epsilon^3\frac{\partial}{\partial x}\left(-2\frac{\partial^2\psi_{\mathrm{T}}}{\partial x\,\partial y}+\ldots\right)+N\epsilon^4\frac{\partial}{\partial y}\left(-2\frac{\partial^2\psi_{\mathrm{T}}}{\partial x\,\partial y}+\ldots\right)\frac{\partial\tilde{\xi}}{\partial x}\\
&\quad=N\epsilon^3\sum_n p_n\,\mathrm{e}^{\mathrm{i}n(x-t)}+O(\epsilon^4)\quad(y=\epsilon\tilde{\zeta}).
\end{aligned}\tag{6.6}$$

The tangential stress boundary condition given in (3.23) can be combined with (5.8) to yield

$$4\frac{\partial^2\psi_{\mathrm{T}}}{\partial x\,\partial y}n_x n_y+\left(\frac{\partial^2\psi_{\mathrm{T}}}{\partial y^2}-\frac{\partial^2\psi_{\mathrm{T}}}{\partial x^2}\right)(n_y n_y-n_x n_x)=\sum_n q_n\,\mathrm{e}^{\mathrm{i}n(x-t)}+O(\epsilon\delta')\quad(y=\epsilon\tilde{\zeta}),\tag{6.7}$$

where the right-hand side is of $O(\delta')$. Recall from (4.2a, b) that the leading-order wave motion is
$$\psi_{\mathrm{T}}=\tfrac{1}{2}A\,\mathrm{e}^{y}\,\mathrm{e}^{\mathrm{i}(x-t)}+*,\tag{6.8}$$
which satisfies (6.6) but not (6.7) to the leading order. Therefore it is necessary to introduce a boundary-layer correction. From the balance of time derivative term and the dissipation term in (6.1), the thickness of the boundary layer is estimated to be $O(\epsilon^{\frac{3}{2}})$. Among the terms on the left-hand side of (6.7), the dominant term in the boundary layer is $\partial^2\psi_{\mathrm{T}}/\partial y^2$ which must be in the same order as the wave motion (6.8) of $O(1)$. This balance is achieved if the boundary-layer correction of ψ_{T} is of $O(\epsilon^3)$. We therefore set
$$\psi_{\mathrm{T}}=\psi+\epsilon^3\psi_{\mathrm{B}},\tag{6.9}$$
where ψ denotes the outer solution and ψ_{B} the boundary-layer correction.

Outside the thin boundary layer, $\psi_{\mathrm{B}}=0$, hence the outer solution ψ must satisfy the same equation (6.1) as ψ_{T}:

$$\nabla^2\frac{\partial\psi}{\partial t}-\epsilon\frac{\partial(\psi,\nabla^2\psi^{\mathrm{S}})}{\partial(x,y)}-\epsilon\frac{\partial(\psi^{\mathrm{S}},\nabla^2\psi)}{\partial(x,y)}-\epsilon\frac{\partial(\psi,\nabla^2\psi)}{\partial(x,y)}-N\epsilon^3\nabla^2\nabla^2\psi=0.\tag{6.10}$$

Consequently, the equation for the boundary-layer correction ψ_{B} reads

$$\begin{aligned}
\nabla^2\frac{\partial\psi_{\mathrm{B}}}{\partial t}-\epsilon\frac{\partial(\psi_{\mathrm{B}},\nabla^2\psi^{\mathrm{S}})}{\partial(x,y)}-\epsilon\frac{\partial(\psi^{\mathrm{S}},\nabla^2\psi_{\mathrm{B}})}{\partial(x,y)}-\epsilon\frac{\partial(\psi_{\mathrm{B}},\nabla^2\psi)}{\partial(x,y)}-\epsilon\frac{\partial(\psi,\nabla^2\psi_{\mathrm{B}})}{\partial(x,y)}\\
-\epsilon^4\frac{\partial(\psi_{\mathrm{B}},\nabla^2\psi_{\mathrm{B}})}{\partial(x,y)}-N\epsilon^3\nabla^2\nabla^2\psi_{\mathrm{B}}=0.
\end{aligned}\tag{6.11}$$

Since the boundary-layer thickness of $O(\epsilon^{\frac{3}{2}})$ is smaller than the wave amplitude of $O(\epsilon)$, it is necessary to introduce a vertical coordinate measured from the free surface:
$$\hat{y}=\frac{y-\epsilon\tilde{\zeta}(x,t)}{\epsilon^{\frac{3}{2}}},\tag{6.12}$$
and set
$$\psi_{\mathrm{B}}=\psi_{\mathrm{B}}(x,\hat{y},t).\tag{6.13}$$

Then the governing equation (6.11) may be simplified to

$$\frac{\partial^2 \psi_B}{\partial t \partial \hat{y}^2} = N \frac{\partial^4 \psi_B}{\partial \hat{y}^4} + O(\epsilon). \tag{6.14}$$

The tangential stress boundary condition (6.7) is now rewritten, within the accuracy of $O(\epsilon, \delta')$, as

$$\left(\frac{\partial^2 \psi_B}{\partial \hat{y}^2}\right)_{\hat{y}=0} + \left(\frac{\partial^2 \psi}{\partial y^2}\right)_{y=0} - \left(\frac{\partial^2 \psi}{\partial x^2}\right)_{y=0} = O(\epsilon, \delta'). \tag{6.15}$$

Introducing the leading-order outer solution (6.8), the boundary condition for the ψ_B is obtained:

$$\frac{\partial^2 \psi_B}{\partial \hat{y}^2} = -A\, e^{i(x-t)} + * \quad (\hat{y} = 0), \tag{6.16}$$

where the right-hand side appears because the leading-order outer solution in water also gives rise to non-zero tangential stress at the surface. The solution of (6.14) which vanishes at $\hat{y} \sim -\infty$ and satisfies (6.16) is

$$\psi_B = -iNA\, e^{i(x-t)} \exp\left(\frac{1-i}{(2N)^{\frac{1}{2}}} \hat{y}\right) + *. \tag{6.17}$$

Introducing (6.9) and (6.17) into (6.4) the kinematic boundary condition for the outer solution ψ on the free surface is obtained:

$$\frac{\partial \tilde{\zeta}}{\partial t} + \epsilon \frac{\partial(\psi + \psi^s)}{\partial y} \frac{\partial \tilde{\zeta}}{\partial x} + \frac{\partial \psi}{\partial x} = -N\epsilon^3 A\, e^{i(x-t)} + * + O(\epsilon^4, \epsilon^3 \delta') \quad (y = \epsilon\tilde{\zeta}). \tag{6.18}$$

Note that the right-hand side is a displacement effect due to the boundary layer correction ψ_B.

Similarly the normal stress boundary condition for ψ can be worked out from (6.6) to be

$$\begin{aligned} &\frac{\partial^2 \psi}{\partial y \partial t} + \epsilon \frac{\partial(\psi + \psi^s)}{\partial y} \frac{\partial^2 \psi}{\partial y \partial x} - \epsilon \frac{\partial \psi}{\partial x} \frac{\partial^2 (\psi + \psi^s)}{\partial y^2} - N\epsilon^3 \nabla^2 \frac{\partial \psi}{\partial y} \\ &\quad + \epsilon \left(-\frac{\partial^2 \psi}{\partial x \partial t} - \epsilon \frac{\partial(\psi + \psi^s)}{\partial y} \frac{\partial^2 \psi}{\partial x^2} + \epsilon \frac{\partial \psi}{\partial x} \frac{\partial^2 \psi}{\partial x \partial y} \right) \frac{\partial \tilde{\zeta}}{\partial x} + \frac{\partial \tilde{\zeta}}{\partial x} - 2N\epsilon^3 \frac{\partial^3 \psi}{\partial x^2 \partial y} \\ &\quad = N\epsilon^3 \sum_n p_n\, e^{in(x-t)} + O(\epsilon^4) \quad (y = \epsilon\tilde{\zeta}), \end{aligned} \tag{6.19}$$

where the effect of ψ_B is at most of $O(\epsilon^4)$ and is neglected.

In summary, the tangential stress due to the leading-order outer wave motion introduces a boundary-layer correction ψ_B, which in turn modifies the surface kinematic boundary condition (6.18) for the outer solution ψ as a displacement thickness. The normal stress due to wind appears as direct forcing on the right-hand side of the boundary condition (6.19). Consequently both normal and tangential stress conditions affect the outer solution ψ, hence contribute to the evolution equation of the wave amplitude A.

In the tangential stress boundary condition (6.7) the effect of wind-induced stress (q_n) appears at the next order $O(\delta', \epsilon)$. The fluctuating parts ($q_n, n \neq 0$) introduce boundary-layer corrections similar to ψ_B, whose displacement effects in (6.18) are at most $O(\epsilon^3 \delta', \epsilon^4)$ and are neglected. On the other hand, it will be shown in §6.3 that the

mean tangential stress q_0 induced by wind and the mean tangential stress induced by waves at the same order modify the basic wind-induced shear s, and introduce in water an additional mean current ψ^q; which affects the phase and the group velocities of water waves.

6.2. *Perturbation analysis of outer solution*

We now start from the governing equation of the outer solution ψ (6.10), and the kinematic and the normal stress boundary conditions (6.18) and (6.19). The motion associated with waves should decay in deep water, hence

$$\psi = 0, \quad y = -\infty. \tag{6.20}$$

Since the left-hand sides of the surface boundary conditions (6.18), (6.19) are functions of ψ and ψ^s which change vertically on the scale of the wavelength, they can be expanded in Taylor series around $y = 0$. (Although the vertical scale of the linear–logarithmic profile ψ^s can be locally smaller than the wavelength, we employ the Taylor expansion including ψ^s. This will be justified when we find in (6.75) that the effects of the wind induced current on the evolution equation (through coefficients κ_{30} and κ_{60}) are numerically small.) The following multiple-scale expansions are then introduced so that at each order the evolution equation of the wave amplitude A is obtained for corresponding time and spatial scales:

$$\left.\begin{aligned} \psi &= \psi_1 + \epsilon\psi_2 + \epsilon^2\psi_3 + \dots, \\ \tilde{\zeta} &= \zeta_1 + \epsilon\zeta_2 + \epsilon^2\zeta_3 + \dots, \end{aligned}\right\} \tag{6.21}$$

where ψ_n, ζ_n depend on $x, x_1, x_2, \dots, y, y_1, y_2, \dots$, and $t, t_1, t_2, \dots$, with $x_n = \epsilon^n x$ etc. Introducing (6.21) into the governing equation and boundary conditions we obtain, at each order, perturbation equations of the general form:

$$\nabla^2 \frac{\partial \psi_n}{\partial t} = F_n, \tag{6.22}$$

$$\frac{\partial \zeta_n}{\partial t} + \frac{\partial \psi_n}{\partial x} = G_n \quad (y = 0), \tag{6.23}$$

$$\frac{\partial^2 \psi_n}{\partial y\, \partial t} + \frac{\partial \zeta_n}{\partial x} = H_n \quad (y = 0), \tag{6.24}$$

$$\psi_n = 0 \quad (y = -\infty), \tag{6.25}$$

for $n \geqslant 1$, where the forcing terms F_n, G_n, and H_n are functions of lower-order solutions. Expanding further in harmonics of progressive waves

$$\begin{Bmatrix} \psi_n \\ \zeta_n \\ F_n \\ G_n \\ H_n \end{Bmatrix} = \sum_m \begin{Bmatrix} \psi_{nm} \\ \zeta_{nm} \\ F_{nm} \\ G_{nm} \\ H_{nm} \end{Bmatrix} e^{im(x-t)} \tag{6.26}$$

we obtain from (6.22)–(6.25)

$$-im\left(\frac{\partial^2 \psi_{nm}}{\partial y^2} - m^2 \psi_{nm}\right) = F_{nm} \tag{6.27}$$

$$-\mathrm{i}m\zeta_{nm}+\mathrm{i}m\psi_{nm}=G_{nm} \quad (y=0) \tag{6.28}$$

$$-\mathrm{i}m\frac{\partial\psi_{nm}}{\partial y}+\mathrm{i}m\zeta_{nm}=H_{nm} \quad (y=0) \tag{6.29}$$

$$\psi_{nm}=0 \quad (y=-\infty). \tag{6.30}$$

At $n=m=1$ the leading-order solutions ψ_{11} and ζ_{11} satisfy the homogeneous governing equation and boundary conditions and have been obtained in (4.1), (6.8)

$$\psi_{11}=\tfrac{1}{2}A\,\mathrm{e}^{y}, \quad \zeta_{11}=\tfrac{1}{2}A. \tag{6.31a, b}$$

Application of Green's identity to ψ_{11} and ψ_{n1} for $n\geqslant 2$ gives

$$\int_{-\infty}^{0}\left[\left(\frac{\partial^2\psi_{n1}}{\partial y^2}-\psi_{n1}\right)\psi_{11}-\left(\frac{\partial^2\psi_{11}}{\partial y^2}-\psi_{11}\right)\psi_{n1}\right]\mathrm{d}y=\int_{-\infty}^{0}\left(-\frac{1}{\mathrm{i}}F_{n1}\psi_{11}\right)\mathrm{d}y \tag{6.32}$$

which is a solvability condition for ψ_{n1}:

$$\int_{-\infty}^{0}F_{n1}\,\mathrm{e}^{y}\,\mathrm{d}y=H_{n1}+G_{n1}. \tag{6.33}$$

Calculations of the forcing terms in (6.27)–(6.29) have been performed by MACSYMA, a symbolic manipulation program. At $n=2$ the forcing terms are calculated to be

$$F_{21}=-\frac{\partial A}{\partial x_1}\mathrm{e}^{y}+\tfrac{1}{2}\mathrm{i}A\,\mathrm{e}^{y}\frac{\partial^3\psi^{\mathrm{s}}}{\partial y^3}, \tag{6.34}$$

$$G_{21}=-\frac{1}{2}\frac{\partial A}{\partial t_1}-\frac{1}{2}\frac{\partial A}{\partial x_1}-\tfrac{1}{2}\mathrm{i}A\left(\frac{\partial\psi^{\mathrm{s}}}{\partial y}\right)_{y=0}, \tag{6.35}$$

$$G_{22}=-\tfrac{1}{2}\mathrm{i}A^2, \tag{6.36}$$

$$H_{21}=-\frac{1}{2}\frac{\partial A}{\partial t_1}-\frac{1}{2}\frac{\partial A}{\partial x_1}-\tfrac{1}{2}\mathrm{i}A\left(\frac{\partial\psi^{\mathrm{s}}}{\partial y}\right)_{y=0}+\tfrac{1}{2}\mathrm{i}A\left(\frac{\partial^2\psi^{\mathrm{s}}}{\partial y^2}\right)_{y=0}, \tag{6.37}$$

$$H_{22}=\tfrac{1}{2}\mathrm{i}A^2, \tag{6.38}$$

$$F_{20}=F_{22}=G_{20}=H_{20}=0. \tag{6.39}$$

The solvability condition of ψ_{21} yields

$$\int_{-\infty}^{0}F_{21}\,\mathrm{e}^{y}\,\mathrm{d}y=H_{21}+G_{21}, \tag{6.40}$$

hence

$$\frac{\partial A}{\partial t_1}+\frac{1}{2}\frac{\partial A}{\partial x_1}+\mathrm{i}A\kappa_{00}=0, \tag{6.41}$$

where

$$\kappa_{00}=\left(\frac{\partial\psi^{\mathrm{s}}}{\partial y}-\frac{1}{2}\frac{\partial^2\psi^{\mathrm{s}}}{\partial y^2}\right)_{y=0}+\int_{-\infty}^{0}\left(\tfrac{1}{2}\mathrm{e}^{2y}\frac{\partial^3\psi^{\mathrm{s}}}{\partial y^3}\right)\mathrm{d}y. \tag{6.42}$$

This is the evolution equation of A in the timescale of $t_1=\epsilon t$. The third term in (6.41) is a Doppler effect resulting from the basic wind induced current ψ^{s} and affects the phase velocity of surface waves at $O(\epsilon)$.

The complete solutions at this order are

$$\psi_{20} = \psi_{20}(x_1, x_2, \ldots, y, y_1, \ldots, t_1, t_2, \ldots), \tag{6.43}$$

$$\psi_{21} = \tfrac{1}{2}\mathrm{i}\frac{\partial A}{\partial x_1}(1-y)\,\mathrm{e}^y + \tfrac{1}{2}\mathrm{i}\frac{\partial A}{\partial t_1}e^y + A\left[g_{00}(y) - \frac{1}{2}\left(\frac{\partial \psi^s}{\partial y}\right)_{y=0}\mathrm{e}^y\right], \tag{6.44}$$

$$\psi_{22} = 0, \tag{6.45}$$

$$\zeta_{20} = \zeta_{20}(x_1, x_2, \ldots, t_1, t_2, \ldots), \tag{6.46}$$

$$\zeta_{21} = 0, \tag{6.47}$$

$$\zeta_{22} = \tfrac{1}{4}A^2, \tag{6.48}$$

where $g_{00}(y)$ is an inhomogeneous solution governed by

$$\frac{\partial^2 g_{00}}{\partial y^2} - g_{00} = -\tfrac{1}{2}\mathrm{e}^y\frac{\partial^3 \psi^s}{\partial y^3} \tag{6.49}$$

with boundary conditions

$$g_{00} = 0, \quad y = 0, -\infty. \tag{6.50}$$

Although an analytical solution is in principle trivial, the solution of $g_{00}(y)$ is obtained numerically for the induced current ψ^s prescribed in (3.20). Note that κ_{00} defined by (6.42) can be rewritten in terms of $g_{00}(y)$:

$$\kappa_{00} = \left(\frac{\partial \psi^s}{\partial y} - \frac{1}{2}\frac{\partial^2 \psi^s}{\partial y^2} + \frac{\partial g_{00}}{\partial y}\right)_{y=0}. \tag{6.51}$$

6.3. *Effect of mean surface tangential stress*

In (5.10) it has been shown that the spatially averaged surface shear stress is modified by q_0 of $O(\epsilon)$, which is the consequence of the nonlinear interaction between wind and waves. The leading-order wave motion (6.8) also introduces a non-zero mean tangential stress at the same order $O(\epsilon)$. Therefore the mean current in water has to be modified accordingly. This modification appears as a part of the stream function ψ_{20}, since it is one order higher than the basic current ψ^s.

Introducing the leading-order solution (6.8) and (4.1) into the tangential stress boundary condition (6.7), and taking the average with respect to x (or t), we obtain

$$\begin{aligned}\epsilon\frac{\partial^2 \psi_{20}}{\partial y^2} &= 4\epsilon\overline{\frac{\partial^2 \psi}{\partial x\,\partial y}\frac{\partial \tilde{\zeta}}{\partial x}} + q_0 + O(\epsilon^2)\\ &= 2\epsilon|A|^2 + q_0 + O(\epsilon^2) \quad (y = \epsilon\tilde{\zeta}),\end{aligned} \tag{6.52}$$

where the overbar denotes time or spatial average. On the right-hand side are the mean surface shear stresses due to wave motion (first term) and due to wind (second term). Since the surface shear q_0 is the result of the nonlinear interaction between surface waves and wind, it is a nonlinear function of wave amplitude $|A|$ once the wind strength u'_*/C is prescribed. It can be inferred from the evolution equation (6.41) that

$$|A| = |A|(x_1 - \tfrac{1}{2}t_1, x_2, x_3, \ldots, t_2, t_3, \ldots), \tag{6.53}$$

because κ_{00} only affects the phase of the complex wave amplitude A. Therefore the forcing q_0 may be written as

$$q_0 = q_0(|A|) = q_0(x_1 - \tfrac{1}{2}t_1, x_2, x_3, \ldots, t_2, t_3, \ldots). \tag{6.54}$$

For convenience we set

$$2\epsilon|A|^2+q_0=\epsilon[q'(x_1-\tfrac{1}{2}t_1,x_2,x_3,\ldots,t_2,t_3,\ldots)+q(x_2,x_3,\ldots,t_2,t_3,\ldots)], \tag{6.55}$$

where ϵq is the average of the left-hand side over x_1 or t_1.

Let us first discuss the effect of the fluctuating part q'. Since it depends on the timescale t_1, the resulting induced current (denoted by $\psi^{q'}$) also depends on t_1. From the balance of the time derivative and dissipative terms in (6.10), $\psi^{q'}$ must decay on the lengthscale of $|y|=O(\epsilon)$, which is comparable to the wave amplitude. Therefore $\psi^{q'}$ is also a boundary-layer correction along the wave surface, similar to ψ_B. The magnitude of $\psi^{q'}$ is estimated to be $O(\epsilon^3)$ since its second derivative in y is $O(\epsilon)$ at the surface. We have shown in §6.1 that the boundary correction ψ_B induces a finite vertical velocity $\partial\psi_B/\partial x$ at the interface and modifies the surface kinematic boundary condition (6.18) of the outer solution ψ. Although $\psi^{q'}$ is comparable with ψ_B in magnitude, its vertical velocity is smaller by $O(\epsilon)$ since it is independent of short scale x. Therefore the effect of $\psi^{q'}$ can be neglected in our analysis.

The remaining part q depends on t_2, t_3 and longer timescales. However, we will later solve the wave amplitude $|A|$ as a function of $\tau=\epsilon^2 t$. Therefore the induced current ψ^q resulting from q is also a function of τ. Let ψ_{20} be further written as

$$\psi_{20}=\psi^q(x_2,x_3,\ldots,y,\tau)+\bar{\psi}_{20}(x_1,x_2,\ldots,y_1,y_2,\ldots,t_1,t_2,\ldots), \tag{6.56}$$

where $\bar{\psi}_{20}$ is shown in Appendix B to be the inviscid wave-induced current. The governing equation of ψ^q is a diffusion equation inferred from (6.10):

$$\frac{\partial^3}{\partial\tau\,\partial y^2}\psi^q=N\epsilon\frac{\partial^4}{\partial y^4}\psi^q, \tag{6.57}$$

where the inertia terms are not important because the forcing q is independent of x or x_1. The surface boundary condition for ψ^q is

$$\frac{\partial^2\psi^q}{\partial y^2}=q \quad (y=0), \tag{6.58}$$

from (6.52) and (6.55). We also impose at infinity

$$\psi^q=0, \quad y=-\infty. \tag{6.59}$$

The solution of (6.57)–(6.59) is simply

$$\frac{\partial^2\psi^q}{\partial y^2}=\frac{-y}{2(N\epsilon\pi)^{\frac{1}{2}}}\int_0^\tau q(\tau-s)\frac{1}{s^{\frac{3}{2}}}\exp\left(-\frac{y^2}{4sN\epsilon}\right)\mathrm{d}s. \tag{6.60}$$

This ψ^q is a modified mean current in water and is a part of ψ_{20}. We stress that ψ^q can be solved only after the history of q (hence that of $|A|$) is numerically calculated.

In summary, to satisfy the tangential stress boundary condition (6.7) to the desired order requires the introduction of the boundary-layer correction ψ_B, and the modified current ψ^q. The effect of ψ_B is to add a displacement in the kinematic boundary condition of outer solution. The modified current ψ^q is a part of the outer solution ψ_{20} and acts as the modification to the basic current ψ^s.

6.4. *Evolution equation for water waves*

The perturbation analysis can now be continued for $n=3$ and 4. While the analysis is similar to existing theories without wind, the details are much lengthier, and are sketched in Appendix B. The solvability condition (6.33) is used to obtain the

evolution equation of wave amplitude A at successive order up to $O(\epsilon^4)$. The results are then combined to yield the equation which is valid up to $\epsilon^3 t = O(1)$:

$$\frac{\partial A}{\partial t_1} + [\tfrac{1}{2} + \epsilon\kappa_{10} + \epsilon^2(\kappa_{11} + \kappa_{50})]\frac{\partial A}{\partial x_1} + \mathrm{i}[\kappa_{00} + \epsilon(\kappa_{01} + \kappa_{20}) + \epsilon^2(\kappa_{02} + \kappa_{21} + \kappa_{40})]A$$

$$+ \mathrm{i}(\epsilon\tfrac{1}{8} + \epsilon^2\kappa_{30})\frac{\partial^2 A}{\partial x_1^2} + \mathrm{i}(\epsilon\tfrac{1}{2} + \epsilon^2\kappa_{60})|A|^2 A - \epsilon^2\frac{1}{16}\frac{\partial^3 A}{\partial x_1^3} + \epsilon^2\tfrac{3}{2}|A|^2\frac{\partial A}{\partial x_1}$$

$$+ \epsilon^2\tfrac{1}{4}A^2\frac{\partial A^*}{\partial x_1} + \epsilon^2\mathrm{i}\left(\frac{\partial \bar{\psi}_{20}}{\partial y_1}\right)_{y_1=0} A + \epsilon^2 2NA - \epsilon^2 N p_1 = 0. \tag{6.61}$$

In the first square bracket κ_{10} and κ_{50} are the modifications of the group velocity due to the basic induced current ψ^s, and κ_{11} is due to the modified current ψ^q given in (6.60). Similarly, modifications of the phase velocity appear in the second square bracket, where κ_{00}, κ_{20}, and κ_{40} are due to ψ^s, and κ_{01} and κ_{21} are due to ψ^q. The effect of ψ_{30} also appears in κ_{02}. The effects of the basic current ψ^s on the linear dispersion (κ_{30}) and on the nonlinear dispersion (κ_{60}) are also present at $O(\epsilon^2)$. All the coefficients (κ) are defined in Appendix B.

For later convenience we rewrite the wind forcing term formally as

$$-\epsilon^2 N p_1 = -\epsilon^2 N(\beta^r + \mathrm{i}\beta^i)A, \tag{6.62}$$

where

$$\beta^r = \frac{1}{2\sigma_e^2}\tilde{\beta}^r, \quad \beta^i = \frac{1}{2\sigma_e^2}\tilde{\beta}^i, \tag{6.63}$$

(cf. (5.14) and (5.15)). The factor $\frac{1}{2}$ appears because β^r is the growth rate of the wave amplitude A whereas the growth rate $\tilde{\beta}^r$ was defined for the wave energy of $O(|A|^2)$. The coefficients β^r and β^i are both of $O(1)$ and are real nonlinear functions of wave slope $ka = \epsilon|A|$ and the normalized friction velocity u'_*/C, calculated numerically in §5. We stress that the explicit dependence of the coefficients β^r, β^i on the wave steepness ka must be kept for consistency, since the nonlinearity in the air flow is not negligible to the leading order in ϵ. The real part β^r and the imaginary part β^i are responsible for the growth and the phase shift of the wave amplitude respectively. Note that if we neglect all κ and set $N = \beta^r = \beta^i = 0$, Dysthe's evolution equation is recovered.

The wave induced current $\bar{\psi}_{20}(x_1, y_1, t_1)$ appearing in (6.61) is governed by the Laplace equation in long scales:

$$\frac{\partial^2 \bar{\psi}_{20}}{\partial x_1^2} + \frac{\partial^2 \bar{\psi}_{20}}{\partial y_1^2} = 0, \tag{6.64}$$

with boundary conditions

$$\frac{\partial \bar{\psi}_{20}}{\partial x_1} = -\frac{1}{2}\frac{\partial |A|^2}{\partial x_1} \quad (y_1 = 0), \tag{6.65}$$

and

$$\bar{\psi}_{20} = 0 \quad (y_1 = -\infty). \tag{6.66}$$

Equation (6.61) together with (6.64)–(6.66) constitute the coupled evolution equations of the wave amplitude A and the wave induced current $\bar{\psi}_{20}$ up to $\epsilon^3 t = O(1)$.

The second and third terms of (6.61) can be eliminated by defining the modified phase velocity $\tilde{c}$ and group velocity $\tilde{c}_g$ due to the wind induced current:

$$\tilde{c} \equiv 1 + \epsilon\tilde{\tilde{c}},$$

with
$$\tilde{\tilde{c}} = \kappa_{00} + \epsilon(\kappa_{01} + \kappa_{20}) + \epsilon^2(\kappa_{02} + \kappa_{21} + \kappa_{40}) + O(\epsilon^3), \tag{6.67}$$

and
$$\tilde{c}_g \equiv \tfrac{1}{2} + \epsilon\kappa_{10} + \epsilon^2(\kappa_{11} + \kappa_{50}) + O(\epsilon^3), \tag{6.68}$$

and introducing the following transformations

$$A = \tilde{A}(\xi, \tau) \exp\left[-\mathrm{i}\int^{t_1} \tilde{\tilde{c}}\,\mathrm{d}t_1\right], \tag{6.69}$$

$$\xi = x_1 - \int^{t_1} \tilde{c}_g\,\mathrm{d}t_1, \quad \tau = \epsilon t_1. \tag{6.70a, b}$$

Equation (6.61) is simplified to

$$\frac{\partial\tilde{A}}{\partial\tau} + \mathrm{i}(\tfrac{1}{8} + \epsilon\kappa_{30})\frac{\partial^2\tilde{A}}{\partial\xi^2} + \mathrm{i}(\tfrac{1}{2} + \epsilon\kappa_{60})|\tilde{A}|^2\tilde{A} - \epsilon\frac{1}{16}\frac{\partial^3\tilde{A}}{\partial\xi^3} + \epsilon\tfrac{3}{2}|\tilde{A}|^2\frac{\partial\tilde{A}}{\partial\xi} + \epsilon\tfrac{1}{4}\tilde{A}^2\frac{\partial\tilde{A}^*}{\partial\xi}$$
$$+ \mathrm{i}\epsilon\left(\frac{\partial\bar{\psi}_{20}}{\partial y_1}\right)_{y_1=0}\tilde{A} - \epsilon N(\beta^r - 2 + \mathrm{i}\beta^i)\tilde{A} = 0, \tag{6.71}$$

where κ_{30}, κ_{60}, defined by (B 52) and (B 55) in Appendix B, are functions of the basic shear ψ^s, and β^r, β^i are functions of the wind strength and the wave amplitude $|\tilde{A}|$. The governing equations for $\bar{\psi}_{20}$ become

$$\frac{\partial^2\bar{\psi}_{20}}{\partial\xi^2} + \frac{\partial^2\bar{\psi}_{20}}{\partial y_1^2} = 0, \tag{6.72}$$

$$\frac{\partial\bar{\psi}_{20}}{\partial\xi} = -\frac{1}{2}\frac{\partial|\tilde{A}|^2}{\partial\xi} \quad (y_1 = 0), \tag{6.73}$$

$$\bar{\psi}_{20} = 0 \quad (y_1 = -\infty). \tag{6.74}$$

Note that the effect of the modified current ψ^q appears only in the phase velocity $\tilde{c}$ and the group velocity $\tilde{c}_g$. As far as the evolution equations (6.71)–(6.74) are concerned, only the effects of the basic shear ψ^s appear through κ_{30} and κ_{60}.

As in the study by Lo & Mei (1985), the fourth, the fifth, and the sixth terms in the evolution equation (6.71) are asymmetric in ξ and all the other terms are symmetric. An initially symmetric profile of $\tilde{A}$ will not remain symmetric over the timescale of $\epsilon\tau = O(1)$.

We now examine the coefficients κ_{30} and κ_{60} which affects the dispersion of the wave amplitude $\tilde{A}$. They are proportional to the basic wind induced current ψ^s and calculated numerically (see Appendix B, equations (B 52), (B 55)) to be

$$\left.\begin{aligned}\epsilon\kappa_{30} &= -0.0337s,\\ \epsilon\kappa_{60} &= -0.1303s.\end{aligned}\right\} \tag{6.75}$$

Both $\epsilon\kappa_{30}$ and $\epsilon\kappa_{60}$ are the products of the normalized wind shear s and a small numerical factor.

In principle, the coefficients κ_{00}, κ_{20}, κ_{40}, in the phase velocity (6.67) and κ_{10}, κ_{50} in the group velocity (6.68) can also be calculated from ψ^s. To solve for the coefficients κ_{01}, κ_{11}, κ_{21} we need the information of ψ^q, hence that of the modified surface shear

q_0 which depends in turn on the history of the wave amplitude $|\tilde{A}|$. Therefore they can be obtained only after the nonlinear evolution equations (6.71)–(6.74) are solved for $\tilde{A}$ as a function of τ. We also note that to calculate the phase velocity $\tilde{c}$ up to $O(\epsilon^3)$, κ_{02} has to be obtained, which depends on the higher-order analysis of air flow. Fortunately, we need not pursue these coefficients here because the evolution of the wave amplitude $|A| = |\tilde{A}|$ in terms of ξ and τ (cf. (6.69)) can be solved without the information of the phase velocity $\tilde{c}$ or the group velocity $\tilde{c}_g$. Equation (6.60) is not evaluated numerically.

7. Initial growth rate of Benjamin–Feir instability

7.1. *Initial growth rate*

In the previous sections the evolution equations (6.71)–(6.74) have been derived, and the coefficients κ_{30}, κ_{60}, β^r, β^i have been computed for various wind conditions. We now study the modulational (Benjamin–Feir) instability of a uniform wavetrain based on these results.

Uniform wavetrain

By setting $\partial/\partial\xi = 0$ in (6.71), we obtain

$$\frac{\partial\tilde{A}}{\partial\tau} + \mathrm{i}(\tfrac{1}{2} + \epsilon\kappa_{60})|\tilde{A}|^2\tilde{A} - \epsilon N(\beta^r - 2)\tilde{A} - \mathrm{i}\epsilon N\beta^i\tilde{A} = 0, \tag{7.1}$$

$$\bar{\psi}_{20} = 0. \tag{7.2}$$

Let
$$\tilde{A} = B\mathrm{e}^{\mathrm{i}\tilde{D}}, \tag{7.3}$$

where B and $\tilde{D}$ are the amplitude and the phase of the complex wave amplitude $\tilde{A}$. Then the real part of (7.1) gives

$$\frac{\partial B}{\partial\tau} - \epsilon N[\beta^r(B) - 2]B = 0, \tag{7.4}$$

and the imaginary part

$$\frac{\partial\tilde{D}}{\partial\tau} + (\tfrac{1}{2} + \epsilon\kappa_{60})B^2 - \epsilon N\beta^i(B) = 0, \tag{7.5}$$

where β^r and β^i are nonlinear functions of B known only numerically. Equation (7.4) solves the evolution of the absolute wave amplitude B. In particular, B only changes over the timescale of $\epsilon\tau = t_3$. The result is then introduced in (7.5) to obtain the phase $\tilde{D}$

$$\tilde{D} = \int_0^\tau [(\tfrac{1}{2} + \epsilon\kappa_{60})B^2 - \epsilon N\beta^i(B)]\,\mathrm{d}\tau + \tilde{D}(\tau = 0). \tag{7.6}$$

We now define a_0 to be the dimensional amplitude of the initial wavetrain. Then from our definition of ϵ (3.15),

$$|\tilde{A}| = B = 1, \quad \text{when } \tau = 0. \tag{7.7}$$

With moderate wind, B eventually approaches to B_{eq} where the wind energy input balances the dissipation due to turbulence in water (i.e. B_{eq} is the solution of $\beta^r(B) = 2$). For stronger wind, B continues to grow since the wind input always surpasses damping. If the wind is so weak that the initial linear growth rate is smaller than the dissipation rate, B gradually decays to zero.

Benjamin–Feir instability

Let
$$\tilde{A} = A_0(1+A'), \quad \bar{\psi}_{20} = \bar{\psi}'_{20}, \tag{7.8}$$

where A_0 is the uniform wavetrain solution, and A', $\bar{\psi}'_{20}$ are small perturbations. Introducing (7.8) into (6.71) and neglecting the terms of $O(A')^2$, we obtain the linearized equation of A':

$$\frac{\partial A'}{\partial \tau} + \mathrm{i}(\tfrac{1}{8}+\epsilon\kappa_{30})\frac{\partial^2 A'}{\partial \xi^2} + \mathrm{i}(\tfrac{1}{2}+\epsilon\kappa_{60})|A_0|^2(A'+A'^*) - \epsilon\frac{1}{16}\frac{\partial^3 A'}{\partial \xi^3} + \epsilon^{\frac{3}{2}}|A_0|^2\frac{\partial A'}{\partial \xi}$$
$$+ \epsilon^{\frac{1}{4}}|A_0|^2\frac{\partial A'^*}{\partial \xi} + \epsilon\mathrm{i}\left(\frac{\partial \bar{\psi}'_{20}}{\partial y_1}\right)_{y_1=0} - \epsilon N^{\frac{1}{2}}\left(\frac{\mathrm{d}\beta^{\mathrm{r}}}{\mathrm{d}B}\right)_{B=|A_0|}|A_0|(A'+A'^*)$$
$$- \mathrm{i}\epsilon N^{\frac{1}{2}}\left(\frac{\mathrm{d}\beta^{\mathrm{i}}}{\mathrm{d}B}\right)_{B=|A_0|}|A_0|(A'+A'^*) = 0, \tag{7.9}$$

and the long wave perturbation $\bar{\psi}'_{20}$ is governed by

$$\frac{\partial^2 \bar{\psi}'_{20}}{\partial \xi^2} + \frac{\partial^2 \bar{\psi}'_{20}}{\partial y_1^2} = 0, \tag{7.10}$$

$$\frac{\partial \bar{\psi}'_{20}}{\partial \xi} = -\tfrac{1}{2}|A_0|^2\frac{\partial}{\partial \xi}(A'+A'^*) \quad (y_1 = 0), \tag{7.11}$$

$$\bar{\psi}'_{20} = 0 \quad (y_1 = -\infty). \tag{7.12}$$

Let A' be separated into real and imaginary parts

$$A' = B_{\mathrm{r}} + \mathrm{i}B_{\mathrm{i}}. \tag{7.13}$$

Then the real part of (7.9) gives

$$\frac{\partial B_{\mathrm{r}}}{\partial \tau} - (\tfrac{1}{8}+\epsilon\kappa_{30})\frac{\partial^2 B_{\mathrm{i}}}{\partial \xi^2} - \epsilon\tfrac{1}{16}\frac{\partial^3 B_{\mathrm{r}}}{\partial \xi^3} + \epsilon^{\frac{3}{2}}|A_0|^2\frac{\partial B_{\mathrm{r}}}{\partial \xi} + \epsilon^{\frac{1}{4}}|A_0|^2\frac{\partial B_{\mathrm{r}}}{\partial \xi} - \epsilon N^{\frac{1}{2}}\left(\frac{\mathrm{d}\beta^{\mathrm{r}}}{\mathrm{d}B}\right)_{B=|A_0|}|A_0|\,2B_{\mathrm{r}} = 0, \tag{7.14}$$

and the imaginary part gives

$$\frac{\partial B_{\mathrm{i}}}{\partial \tau} + (\tfrac{1}{8}+\epsilon\kappa_{30})\frac{\partial^2 B_{\mathrm{r}}}{\partial \xi^2} + (\tfrac{1}{2}+\epsilon\kappa_{60})|A_0|^2\,2B_{\mathrm{r}} - \epsilon\frac{1}{16}\frac{\partial^3 B_{\mathrm{i}}}{\partial \xi^3} + \epsilon^{\frac{3}{2}}|A_0|^2\frac{\partial B_{\mathrm{i}}}{\partial \xi}$$
$$- \epsilon^{\frac{1}{4}}|A_0|^2\frac{\partial B_{\mathrm{i}}}{\partial \xi} + \epsilon\left(\frac{\partial \bar{\psi}'_{20}}{\partial y_1}\right)_{y_1=0} - \epsilon N^{\frac{1}{2}}\left(\frac{\mathrm{d}\beta^{\mathrm{i}}}{\mathrm{d}B}\right)_{B=|A_0|}|A_0|\,2B_{\mathrm{r}} = 0. \tag{7.15}$$

In the initial growth stage of the disturbances, A_0 is assumed to be approximately constant with unit magnitude, since it is a function of $\epsilon\tau = t_3$. Therefore we may introduce

$$B_{\mathrm{r}} = b_{\mathrm{r}}\mathrm{e}^{\mathrm{i}(K\xi-\Omega\tau)}, \quad B_{\mathrm{i}} = b_{\mathrm{i}}\mathrm{e}^{\mathrm{i}(K\xi-\Omega\tau)}, \tag{7.16a, b}$$

where $K > 0$ is the wavenumber of the disturbances, and Ω is the complex frequency. From (7.10)–(7.12) the solution of $\bar{\psi}'_{20}$ is obtained as

$$\bar{\psi}'_{20} = -b_{\mathrm{r}}\exp(Ky_1)\exp[\mathrm{i}(K\xi-\Omega\tau)], \tag{7.17}$$

and
$$\left(\frac{\partial \bar{\psi}'_{20}}{\partial y_1}\right)_{y_1=0} = -b_{\mathrm{r}}K\,\mathrm{e}^{\mathrm{i}(K\xi-\Omega\tau)}. \tag{7.18}$$

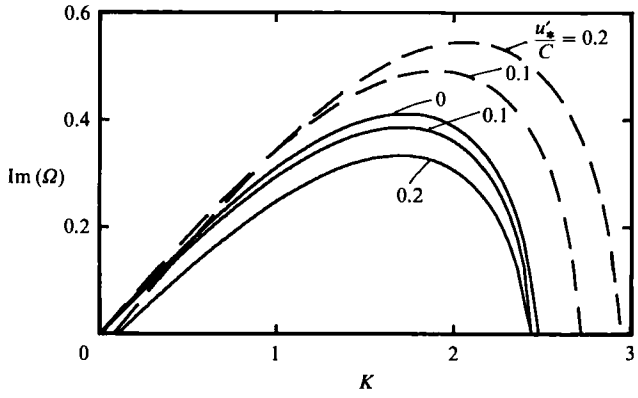

FIGURE 5. Instability growth rate $\mathrm{Im}(\Omega)$ as a function of wave number K for various values of normalized friction velocity u'_*/C. $\epsilon = 0.1$. ——, Linear–logarithmic current profile; – –, linear current profile in water.

Introducing (7.16) and (7.18) into (7.14) and (7.15) we obtain two homogeneous algebraic equations for b_r and b_i:

$$\left[-\mathrm{i}\Omega + \tfrac{1}{16}\mathrm{i}\epsilon K^3 + \tfrac{3}{2}\mathrm{i}\epsilon K + \tfrac{1}{4}\mathrm{i}\epsilon K - \epsilon N\left(\frac{\mathrm{d}\beta^r}{\mathrm{d}B}\right)_{B=1}\right] b_r + [(\tfrac{1}{8} + \epsilon\kappa_{30})K^2]\, b_i = 0, \tag{7.19}$$

$$\left[-(\tfrac{1}{8} + \epsilon\kappa_{30})K^2 + 2(\tfrac{1}{2} + \epsilon\kappa_{60}) - \epsilon K - \epsilon N\left(\frac{\mathrm{d}\beta^i}{\mathrm{d}B}\right)_{B=1}\right] b_r + (-\mathrm{i}\Omega + \tfrac{1}{16}\mathrm{i}\epsilon K^3 + \tfrac{3}{2}\mathrm{i}\epsilon K - \tfrac{1}{4}\mathrm{i}\epsilon NK)\, b_i = 0, \tag{7.20}$$

for which a non-trivial solution exists only when

$$\Omega = \frac{1}{2}\left[\tfrac{1}{8}\epsilon K^3 + 3\epsilon K + \mathrm{i}\epsilon N\left(\frac{\mathrm{d}\beta^r}{\mathrm{d}B}\right)_{B=1}\right] \pm \frac{1}{2}\left\{-\epsilon^2 N^2\left(\frac{\mathrm{d}\beta^r}{\mathrm{d}B}\right)^2_{B=1} + \tfrac{1}{4}\epsilon^2 K^2 + \mathrm{i}\epsilon^2 N\left(\frac{\mathrm{d}\beta^r}{\mathrm{d}B}\right)_{B=1} K - 4\left[-(\tfrac{1}{8} + \epsilon\kappa_{30})K^2 + 2(\tfrac{1}{2} + \epsilon\kappa_{60}) - \epsilon K - \epsilon N\left(\frac{\mathrm{d}\beta^i}{\mathrm{d}B}\right)_{B=1}\right][(\tfrac{1}{8} + \epsilon\kappa_{30})K^2]\right\}^{\frac{1}{2}}, \tag{7.21}$$

or

$$\Omega = \frac{1}{2}\left[\tfrac{1}{8}\epsilon K^3 + 3\epsilon K + \mathrm{i}\epsilon N\left(\frac{\mathrm{d}\beta^r}{\mathrm{d}B}\right)_{B=1}\right] \pm \left[(\tfrac{1}{64} + \tfrac{1}{4}\epsilon\kappa_{30})K^4 - 2K^2(\tfrac{1}{16} + \tfrac{1}{2}\epsilon\kappa_{30} + \tfrac{1}{8}\epsilon\kappa_{60}) + \tfrac{1}{8}\epsilon K^3 + \tfrac{1}{8}\epsilon NK^2\left(\frac{\mathrm{d}\beta^i}{\mathrm{d}B}\right)_{B=1}\right]^{\frac{1}{2}}, \tag{7.22}$$

to the accuracy of $O(\epsilon)$. For instability $\mathrm{Im}(\Omega) > 0$.

In the case of no wind or damping ($N = \beta^r = \beta^i = \kappa_{30} = \kappa_{60} = 0$), Dysthe's result is recovered:

$$\Omega = \tfrac{1}{16}\epsilon K^3 + \tfrac{3}{2}\epsilon K \pm (\tfrac{1}{64}K^4 - \tfrac{1}{8}K^2 + \tfrac{1}{8}\epsilon K^3)^{\frac{1}{2}}. \tag{7.23}$$

7.2. *Discussion of results*

In figure 5 we plot the initial growth of an unstable disturbance for a fixed wave slope $\epsilon = 0.1$ and for various wind speeds $u'_*/C = 0$, 0.1, 0.2 by solid lines. The instability is slightly suppressed as the normalized friction velocity increases. We have also assumed other profiles for the wind-induced water shear and have found that the

u'_*/C	k (cm^{-1})	ϵ	Γ_M (m^{-1})	$\Delta f/f$
0	0.161	0.219	0.497	0.157
0.217	0.146	0.203	0.296	0.159
0.286	0.142	0.210	0.275	0.163
0.316	0.140	0.214	0.267	0.166

TABLE 2. Instability growth rate and relative modulational frequency

initial growth rate can be quite different, since the term κ_{60} in (7.22) changes significantly for different current profiles. For example, if the profile is linear instead of linear–logarithmic, the instability is then greatly enhanced as is also shown in figure 5 by broken lines. Li *et al.* (1987) also found a similar trend with the same linear current profile when wind was relatively weak, although they assumed much stronger wind and neglected the direct effects of surface stresses due to wind. We have also examined an error function profile which is the exact solution of the Reynolds equations with the constant eddy viscosity. The effect is then to suppress the instability even more strongly. Based on these observations, precise knowledge of the induced turbulent current is essential to estimate the growth rate accurately.

7.3. *Comparison of theory with available experimental data*

Bliven *et al.* (1986) studied experimentally the growth rate of Benjamin–Feir instability of mechanically driven waves under the influence of wind. For the initial wave steepness $\epsilon \approx 0.22$ and the wave frequency $f = 2$ Hz, the instability growth rate is reduced significantly when u'_*/C is increased from 0 to 0.43. They also found that the bandwidth of the frequency modulation is increased. Since their measurements give instability growth rates in space rather than in time, it is necessary to translate our calculated time growth rates into spatial growth rates for comparison. Note that our theory was constructed in the frame of reference following the surface drift velocity $u_{\rm d}$ which was left undetermined. Now for comparison with experiments, it is necessary to give a specific value of $u_{\rm d}$. Unfortunately, the surface drift was not measured in Bliven *et al.* We therefore estimate it by using Wu's (1975) empirical formula

$$u_{\rm d} = 0.55\frac{u'_*}{C}. \tag{7.24}$$

This surface drift modifies not only the group velocity $\tilde{c}_{\rm g}$ but also the phase velocity $\tilde{c}$ according to $2\pi f/(gk)^{\frac{1}{2}} = \tilde{c}+u_{\rm d}$. As a result, the actual wavenumber in the experiments is slightly decreased by a factor of $1/(\tilde{c}+u_{\rm d})^2$ compared with the value calculated by Bliven *et al.* from only the leading-order dispersion relationship. We first estimate the actual wavenumber k for each case of their experiments as shown in table 2. The dimensional spatial growth rate Γ is then given as

$$\Gamma = k\epsilon^2\frac{\mathrm{Im}\,(\Omega)}{(\tilde{c}_{\rm g}+u_{\rm d})}. \tag{7.25}$$

Once the maximum growth rate Γ_M and the corresponding disturbance wavenumber K_M are solved, the relative width of the frequency modulation $\Delta f/f$ can be calculated as

$$\frac{\Delta f}{f} = \epsilon K_M\frac{\tilde{c}_{\rm g}+u_{\rm d}}{\tilde{c}+u_{\rm d}}. \tag{7.26}$$

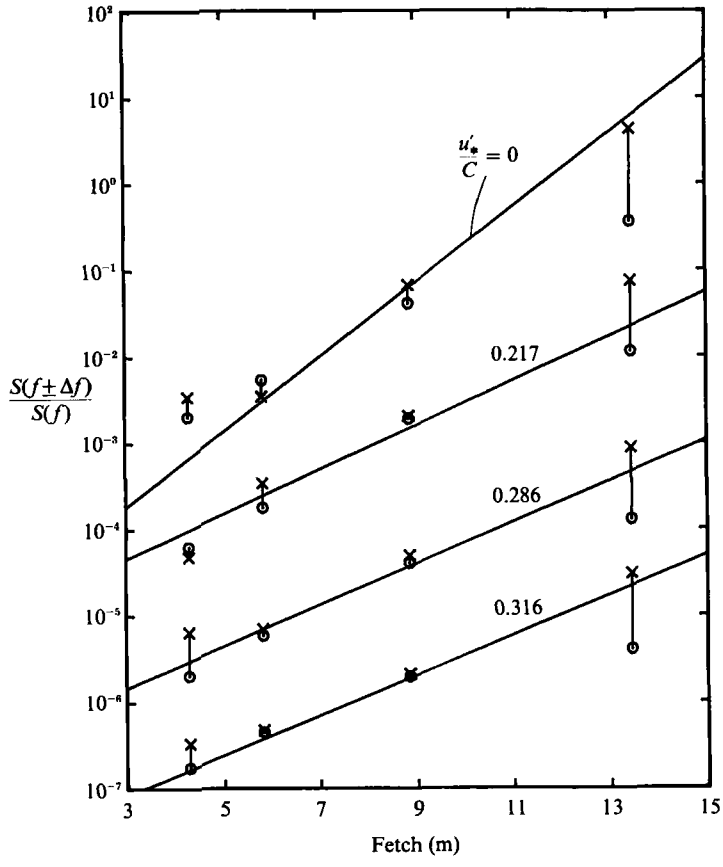

FIGURE 6. Ratio of frequency spectrum of sidebands to that of fundamental frequency as functions of fetch. ○, upper sideband; ×, lower sideband (Bliven *et al.* 1986); ——, Our calculation. Results for $u'_*/C = 0.217, 0.286, 0.316$ are shifted by 10^{-1}, 10^{-2}, 10^{-3} respectively.

The phase velocity $\tilde{c}$ and the group velocity $\tilde{c}_g$ may be approximated by

$$\tilde{c} = 1+\epsilon\kappa_{00} = 1-0.1848s = 1-0.322\frac{u'_*}{C}, \tag{7.27}$$

$$\tilde{c}_g = 0.5+\epsilon\kappa_{10} = 0.5-0.1221s = 0.5-0.213\frac{u'_*}{C}, \tag{7.28}$$

(cf. (6.67) and (6.68)), where κ_{00} and κ_{10} are calculated from (6.51) and (B 34) using our basic linear–logarithmic current profile (3.20).

The numerical results of Γ_M and $\Delta f/f$ are shown in table 2 for the four experiments. The values of the initial wave steepness ϵ are determined from the wave amplitude data at the first wave gauge (fetch 4.29 m) and our estimated wavenumber k.

We estimate the ratios of the frequency spectrum of the upper and lower sidebands to that of the fundamental frequency from figures 1 and 4 of Bliven *et al.* and plot in figure 6 as functions of fetch. The growth rates based on our calculations are also shown by solid lines. Both results clearly indicate the suppression of the sideband instability due to wind. The agreement between them is fair, although the wave steepness and the wind strength are both slightly beyond the validity of our theory.

In the experiments the relative modulational frequency $\Delta f/f$ (i.e. the separation between the sidebands) increases from 0.15 to 0.28 as the wind increases from $u'_*/C = 0$ to 0.316, whereas our calculation gives a much slower increase from 0.157 to 0.166. The reason of this discrepancy is not clear. We have also examined the linear water current profile. The instability growth rate then increases by 200% with the strongest wind, which is qualitatively opposite to the experimental results. Therefore the log–linear current profile is kept for the remainder of this paper.

Finally, we comment on the effect of the eddy viscosity ν_e in water on the initial growth rate. When ν_e is decreased, both the instability growth rate and the separation of the two sidebands are significantly reduced to the strong wind-induced current (large s), resulting in poorer agreement with the experiments. On the other hand, the initial instability is relatively insensitive to the increase of the eddy viscosity because the Doppler shift by the surface drift u_d remains the same and dominant. Note, however, that the linear wave growth rate due to wind (figure 1) is reduced by larger eddy viscosity and further deviates from the experimental data for a relatively weak wind (around $u'_*/C = 0.1$). These facts suggest that our choice of the constant eddy viscosity ν_e is appropriate at least in order of magnitude.

8. Nonlinear evolution of instability

In this section we shall examine the long-time evolution of the Benjamin–Feir instability under wind, where relatively small wave amplitude and weak wind are chosen so that the effect of breaking is insignificant.

8.1. *Numerical method of solution*

Starting from the initial growth rate in §7 we now examine the nonlinear evolution of Benjamin–Feir instability by solving (6.71)–(6.74) numerically. First, the least stable wavenumber K and the corresponding Ω are obtained from (7.22) for prescribed initial wave slope ϵ and normalized friction velocity u'_*/C. The result is then introduced to (7.19) or (7.20) to calculate b_i/b_r. The initial condition of the disturbance A' at $\tau = 0$ is then

$$\begin{aligned} A' &= B_r + iB_i \\ &= \tfrac{1}{2}(b_r e^{iK\xi} + *) + \tfrac{1}{2}i(b_i e^{iK\xi} + *) \\ &= \tfrac{1}{2}b_r\left(1 + i\frac{b_i}{b_r}\right)e^{iK\xi} + \tfrac{1}{2}b_r^*\left(1 + i\frac{b_i^*}{b_r^*}\right)e^{-iK\xi}. \end{aligned} \tag{8.1}$$

Although $|b_r|$ has been assumed to be infinitesimal in §7, we now set

$$b_r = 0.1 \times \left[\left|\frac{1}{2}\left(1 + i\frac{b_i}{b_r}\right)\right| + \left|\frac{1}{2}\left(1 + i\frac{b_i^*}{b_r^*}\right|\right]^{-1}, \tag{8.2}$$

so that the maximum of $|A'|$ is 0.1. The computed initial condition for $\tilde{A}$ is then

$$\begin{aligned} \tilde{A} = 1 + 0.1 \times &\left[\frac{1}{2}\left(1 + i\frac{b_i}{b_r}\right)e^{iK\xi} + \frac{1}{2}\left(1 + i\frac{b_i^*}{b_r^*}\right)e^{-iK\xi}\right] \\ &\times \left[\left|\frac{1}{2}\left(1 + i\frac{b_i}{b_r}\right)\right| + \left|\frac{1}{2}\left(1 + i\frac{b_i^*}{b_r^*}\right)\right|\right]^{-1} \quad (\tau = 0). \end{aligned} \tag{8.3}$$

If the initial amplitude of the disturbance is reduced, the initial growth is delayed but the subsequent evolution remains similar.

The pseudo-spectral method for solving (6.71)–(6.74) is identical to that of Lo & Mei (1985), where the nonlinear part is integrated in the physical domain and the linear part in the frequency domain. Let us introduce $M = 2^m$ (m = integer) equally spaced grid points between $\tilde{\xi} \equiv K\xi = 0$ and $\tilde{\xi} = 2\pi$:

$$\tilde{\xi}_0 = 0, \quad \tilde{\xi}_1 = \frac{2\pi}{M}, \quad \tilde{\xi}_2 = \frac{4\pi}{M}, \ldots, \quad \tilde{\xi}_{M-1} = \frac{2(M-1)\pi}{M}, \quad \tilde{\xi}_M = 2\pi, \tag{8.4}$$

and define

$$\tilde{A}_n \equiv \tilde{A}(\tilde{\xi} = \tilde{\xi}_n). \tag{8.5}$$

The Fourier transform of $\tilde{A}$ is given as

$$B_\nu = \frac{1}{M} \sum_{n=0}^{M-1} \tilde{A}_n \exp(-\mathrm{i}\nu\tilde{\xi}_n), \quad B_{\nu+M} = B_\nu, \tag{8.6}$$

and the inverse Fourier transform as

$$\tilde{A}_n = \sum_{\nu=0}^{M-1} B_\nu \exp(\mathrm{i}\nu\tilde{\xi}_n) = \sum_{\nu=-\frac{1}{2}M+1}^{\frac{1}{2}M} B_\nu \exp(\mathrm{i}\nu\tilde{\xi}_n). \tag{8.7}$$

We separate (6.71) into linear and nonlinear parts. First, the nonlinear part is integrated by the modified Euler scheme in the physical domain, then the linear part is integrated exactly in the Fourier domain. In the next timestep the linear part is calculated first and the nonlinear part second. In this manner a global accuracy of $O(\Delta\tau)^2$ can be achieved. To avoid aliasing errors due to nonlinearity, we use twice the number of points in the linear integration, as is suggested by Lo & Mei (1985).

As the integration proceeds, we have found that one particular high harmonic is excited and the profile of $|\tilde{A}|$ becomes highly oscillatory with the corresponding frequency. This happens because the ξ-derivatives ($\partial^2/\partial\xi^2, \partial^3/\partial\xi^3$) of the high harmonic become quite large and may balance with the lower-order terms which should be $O(1/\epsilon)$ times larger. In the evolution equation (6.71), the following two terms,

$$+\mathrm{i}(\tfrac{1}{8}+\epsilon\kappa_{30})\frac{\partial^2\tilde{A}}{\partial\xi^2} - \epsilon\frac{1}{16}\frac{\partial^3\tilde{A}}{\partial\xi^3}, \tag{8.8}$$

become dominant, which corresponds to

$$\sum_{\nu=-\frac{1}{2}M+1}^{\frac{1}{2}M} [+\mathrm{i}(\tfrac{1}{8}+\epsilon\kappa_{30})(\mathrm{i}\nu K)^2 B_\nu - \epsilon\tfrac{1}{16}(\mathrm{i}\nu K)^3 B_\nu] \mathrm{e}^{\mathrm{i}\nu\tilde{\xi}} \tag{8.9}$$

in the Fourier domain. These two terms are comparable when

$$-(\tfrac{1}{8})(\nu K)^2 + \epsilon\tfrac{1}{16}(\nu K)^3 \approx 0, \tag{8.10}$$

or

$$\nu \approx \frac{2}{\epsilon K} = O\left(\frac{1}{\epsilon}\right). \tag{8.11}$$

Thus the dominant harmonic has a high frequency of $O(1/\epsilon)$. To overcome this difficulty we include a higher-order dispersive term $\partial^4\tilde{A}/\partial\xi^4$ which is otherwise of

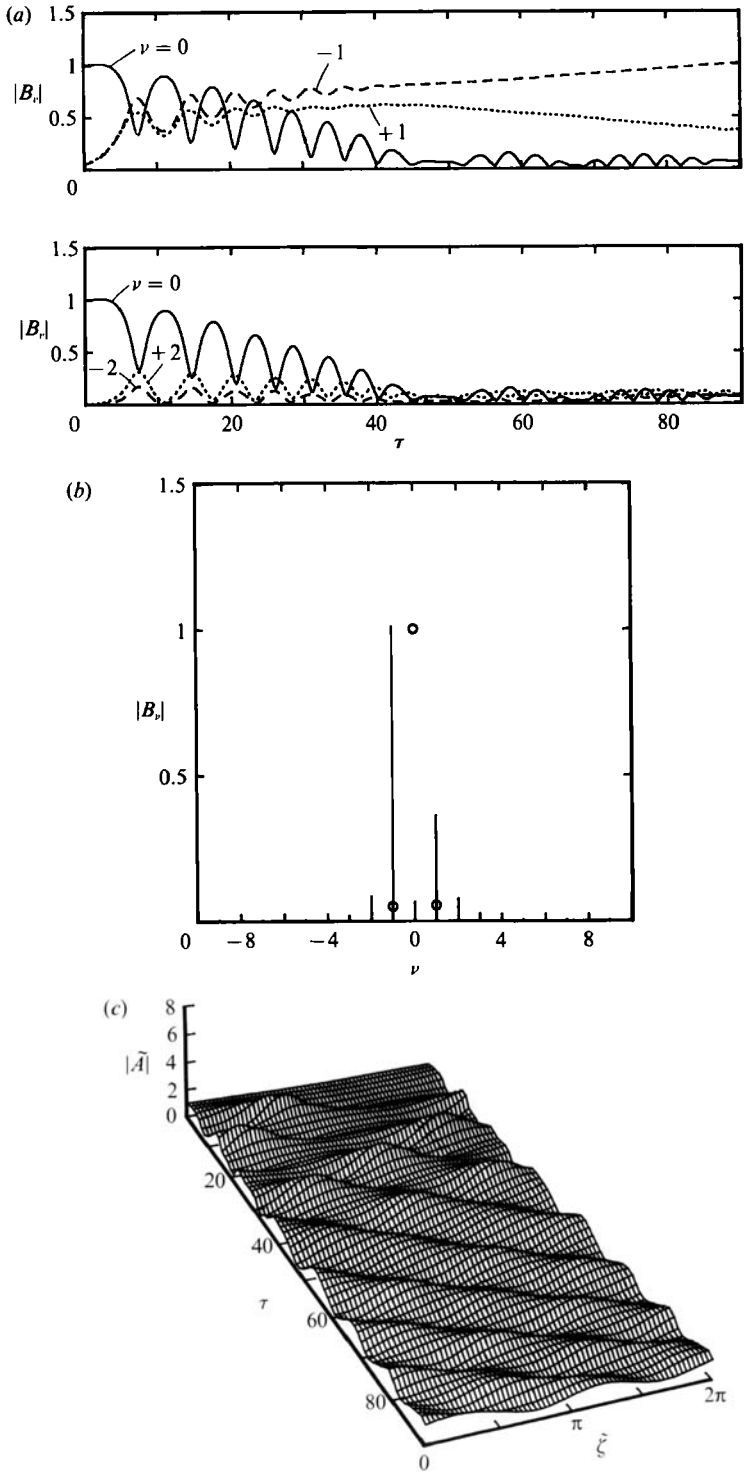

FIGURE 7. (*a*) Time evolution of lowest 5 Fourier components ($|B_\nu|$, $\nu = \pm 2, \pm 1, 0$) of wave amplitude $\tilde{A}$. $u'_*/C = 0.12$, $\epsilon = 0.070$, $K = 1.81$, $\Delta\tau = 0.0026$. (*b*) Amplitude spectrum of wave amplitude $\tilde{A}$ at $\tau = 90$. $u'_*/C = 0.12$, $\epsilon = 0.070$. Circles are spectrum at $\tau = 0$. (*c*) Time evolution of $|\tilde{A}|$. $u'_*/C = 0.12$, $\epsilon = 0.070$.

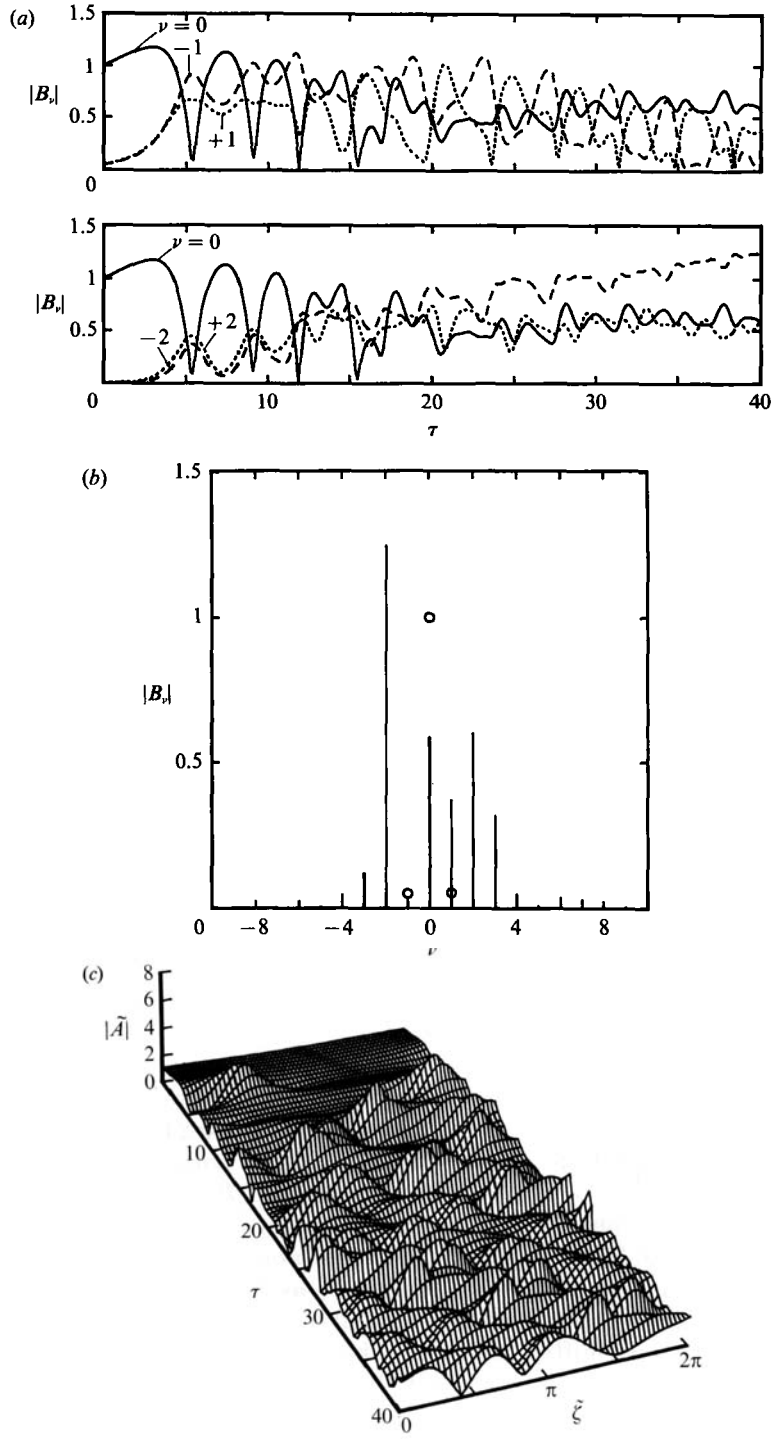

FIGURE 8. (*a*) Time evolution of lowest 5 Fourier components ($|B_\nu|$, $\nu = \pm 2, \pm 1, 0$) of wave amplitude $\tilde{A}$. $u'_*/C = 0.12$, $\epsilon = 0.044$, $K = 1.88$, $\Delta\tau = 0.001$. (*b*) Amplitude spectrum of wave amplitude $\tilde{A}$ at $\tau = 40$. $u'_*/C = 0.12$, $\epsilon = 0.044$. Circles are spectrum at $\tau = 0$. (*c*) Time evolution of $|\tilde{A}|$. $u'_*/C = 0.12$, $\epsilon = 0.044$.

$O(\epsilon^2)$ in the asymptotic equation (6.71). The coefficient of this term may be obtained as

$$-\mathrm{i}\epsilon^2 \frac{5}{128}\frac{\partial^4 \tilde{A}}{\partial \xi^4} \tag{8.12}$$

from the linear dispersive wave theory. With this term the dominant derivative terms are

$$+\mathrm{i}(\tfrac{1}{8}+\epsilon\kappa_{30})\frac{\partial^2 \tilde{A}}{\partial \xi^2}-\epsilon\frac{1}{16}\frac{\partial^3 \tilde{A}}{\partial \xi^3}-\mathrm{i}\epsilon^2\frac{5}{128}\frac{\partial^4 \tilde{A}}{\partial \xi^4}, \tag{8.13}$$

or

$$\sum_{\nu=-\frac{1}{2}M+1}^{\frac{1}{2}M}[+\mathrm{i}(\tfrac{1}{8}+\epsilon\kappa_{30})(\mathrm{i}\nu K)^2 B_\nu-\epsilon\tfrac{1}{16}(\mathrm{i}\nu K)^3 B_\nu-\mathrm{i}\epsilon^2\tfrac{5}{128}(\mathrm{i}\nu K)^4 B_\nu]\,\mathrm{e}^{\mathrm{i}\nu\tilde{\zeta}} \tag{8.14}$$

in the Fourier domain. These three terms would cancel one another only if

$$-(\tfrac{1}{8})(\nu K)^2+\epsilon\tfrac{1}{16}(\nu K)^3-\epsilon^2\tfrac{5}{128}(\nu K)^4 \approx 0, \tag{8.15}$$

which does not have a real solution. Hence no high harmonics will be numerically excited.

8.2. *Results and discussions*

Lo & Mei (1985) have calculated the long-time evolution of the Benjamin–Feir instability according to Dysthe's equations without wind or damping. They have found that a recurrence pattern known in the lower-order Schrödinger equation is still preserved. Near the peak of the modulation the lower sideband becomes slightly larger than the upper sideband, indicating a temporary downshift of frequency. However, the recurrence is nearly periodic; the downshift disappears later and the spectrum goes back to the original.

We now examine three different wind strengths, $u'_*/C = 0.12$, 0.14, and 0.16 ($s' =$ 6, 7 and 8).

8.2.1. $u'_*/C = 0.12$

As indicated by figure 2(*a*), the net growth rate becomes zero at $(ka)_{\mathrm{eq}} = 0.085$. We examine two different initial wave slopes $\epsilon = 0.070$ and 0.044.

Case (i) $\epsilon = 0.070$ $(N = 0.24)$

Referring to (3.15) and the value of the viscosity parameter σ_{e}^2 in table 1, the normalized dissipation coefficient N is calculated to be $N = 0.24$. By definition (4.3) the equilibrium wave amplitude should be $|A|_{\mathrm{eq}} = B_{\mathrm{eq}} = (ka)_{\mathrm{eq}}/\epsilon = 1.22$. In figure 7(*a*) the evolution of the zeroth, $\pm$1st, $\pm$2nd harmonics ($|B_0|, |B_{\pm 1}|, |B_{\pm 2}|$) are shown for $\tau = 0$–90. At the beginning a quasi-recurrence pattern is observed as in the case of Dysthe's equation; the lower sideband ($-$1st harmonic) outgrows the upper side band ($+$1st harmonic) near its peaks. However, as the evolution proceeds the magnitude of all but the $-$1st harmonic gradually decays, and at $\tau = 90$ the peak wavenumber is clearly downshifted to the $-$1st harmonic, implying that there is now a monotonic downshift of frequency peak with time.

In figure 7(*b*) the amplitude spectrum of the harmonics ($|B_\nu|$, $\nu = -10$ to 10) is plotted at $\tau = 90$. The initial spectrum is also indicated by circles. There appears a single peak at $\nu = -1$, and all the other harmonics are relatively small. We also show in figure 7(*c*) the evolution of the wave amplitude profile $|\tilde{A}|$. The strong recurrent modulation in the initial stage gradually gives way to the almost steady superposition of the $\pm$1st harmonics.

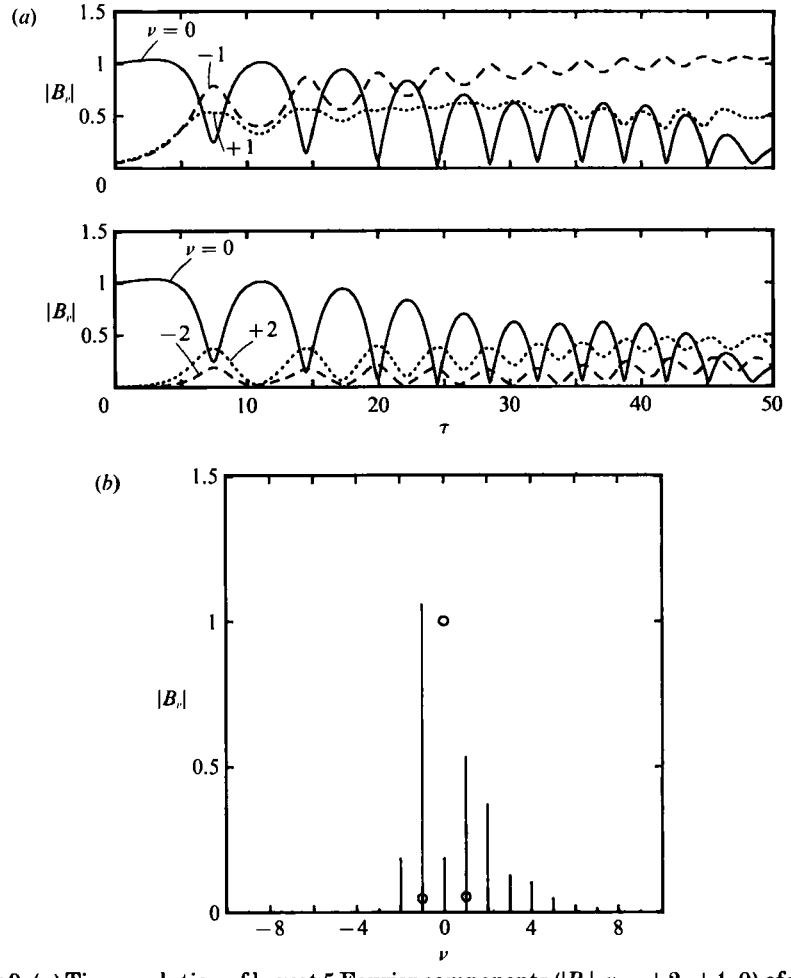

FIGURE 9. (*a*) Time evolution of lowest 5 Fourier components ($|B_\nu|$, $\nu = \pm 2, \pm 1, 0$) of wave amplitude $\tilde{A}$. $u'_*/C = 0.14, \epsilon = 0.092, K = 1.73, \Delta\tau = 0.00167$. (*b*) Amplitude spectrum of wave amplitude $\tilde{A}$ at $\tau = 50$. $u'_*/C = 0.14$, $\epsilon = 0.092$. Circles are spectrum at $\tau = 0$.

Case (ii) $\epsilon = 0.044 \quad (N = 1)$

Next we examine the case of a smaller initial wave amplitude. By definition B_{eq} is now 1.95. Hence the magnitude of the uniform wavetrain will gradually approach 1.95 times the original if the unstable sideband disturbances are not introduced. From the analysis of §7, we find that the dimensional wavenumber of the sideband instability is roughly proportional to the amplitude of the uniform train. Referring to the instability diagram, figure 5, the sideband disturbance of wavenumber up to 1.3–1.4 times that of the least stable mode is unstable at $\tau = 0$. Therefore, for large τ the maximum dimensional unstable wavenumber will be roughly 2.5–2.7 times that of the original least stable wavenumber. In our calculation with discrete Fourier series it may be expected that the Fourier components of the wavenumber twice that of the initial disturbances ($B_{\pm 2}$) will also become unstable for large τ.

The time evolution of the lowest 5 harmonics are plotted in figure 8(*a*). In the initial stage ($\tau \leqslant 15$) a quasi-recurrence pattern is evident and the -1st harmonic slowly grows as in the former case. However, for larger time the evolution pattern

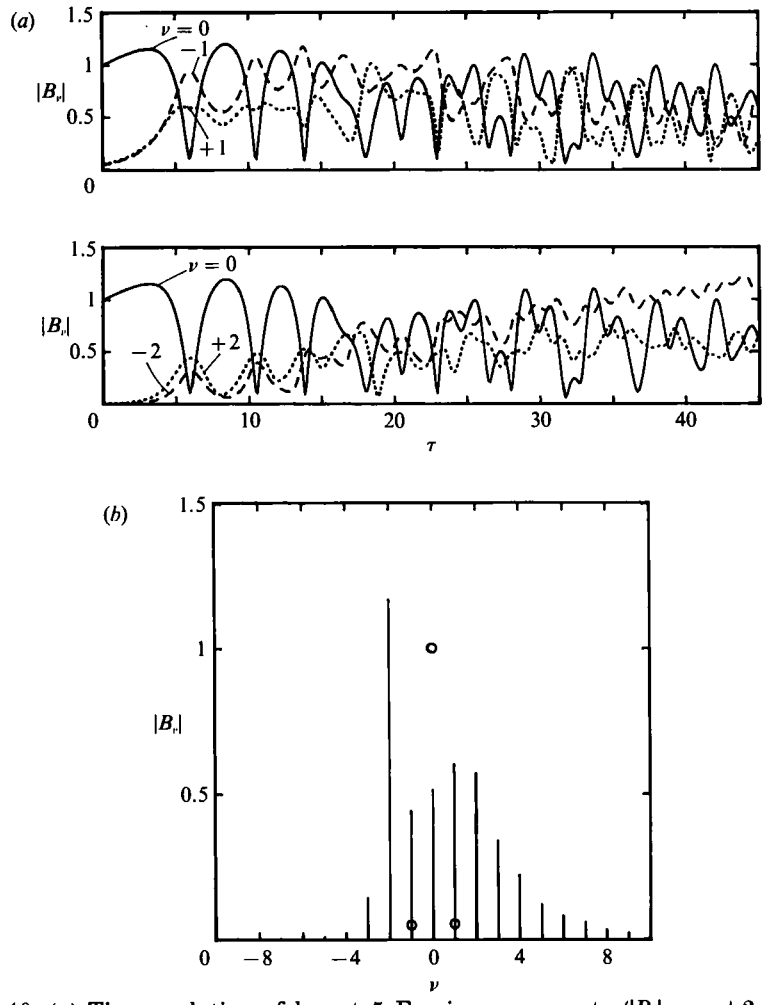

FIGURE 10. (a) Time evolution of lowest 5 Fourier components ($|B_\nu|$, $\nu = \pm 2, \pm 1, 0$) of wave amplitude $\tilde{A}$. $u'_*/C = 0.14$, $\epsilon = 0.069$, $K = 1.81$, $\Delta\tau = 0.00094$. (b) Amplitude spectrum of wave amplitude $\tilde{A}$ at $\tau = 45$. $u'_*/C = 0.14$, $\epsilon = 0.069$. Circles are spectrum at $\tau = 0$.

becomes more chaotic and the -2nd harmonic gradually overtakes the other harmonics to become dominant.

The plot of the final amplitude spectrum figure 8(*b*) at $\tau = 40$ clearly shows the downshift of the peak wavenumber to $\nu = -2$, although some of other harmonics are also not small. This is again clear evidence of the permanent frequency downshift. The profile of the wave amplitude $|\tilde{A}|$ in figure 8(*c*) also shows a rather chaotic evolution pattern for $\tau > 15$.

8.2.2. $u'_*/C = 0.14$

We now examine a slightly stronger wind. Again two different initial wave slopes $\epsilon = 0.092$ and 0.069 are examined.

Case (iii) $\epsilon = 0.092$ $(N = 0.125)$

The time evolution of the lowest 5 harmonics is plotted in figure 9(*a*), and the final amplitude spectrum in figure 9(*b*). As in case (i) the -1st harmonic gradually becomes dominant, although the other harmonics do not decay as quickly as in case

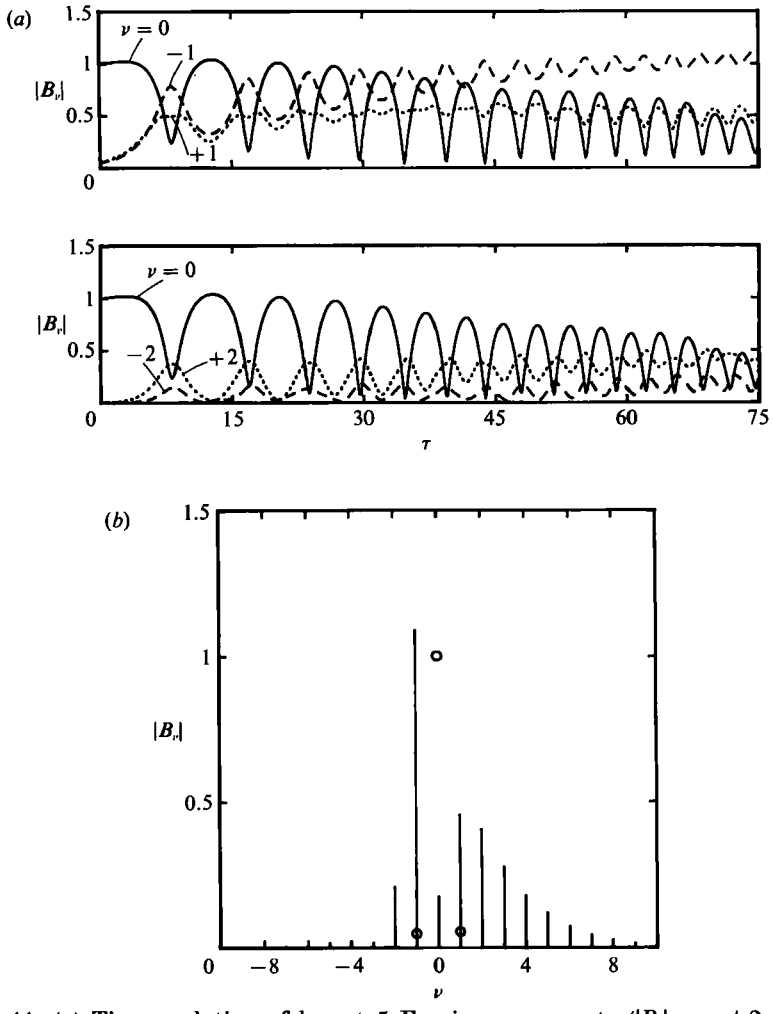

FIGURE 11. (*a*) Time evolution of lowest 5 Fourier components ($|B_\nu|$, $\nu = \pm 2, \pm 1, 0$) of wave amplitude $\tilde{A}$. $u'_*/C = 0.16$, $\epsilon = 0.120$, $K = 1.64$, $\Delta\tau = 0.0026$. (*b*) Amplitude spectrum of wave amplitude $\tilde{A}$ at $\tau = 75$. $u'_*/C = 0.16$, $\epsilon = 0.120$. Circles are spectrum at $\tau = 0$.

(i) and quasi-recurrence persists for a much longer time. The amplitude spectrum at $\tau = 50$ again shows the tendency of a monotonic frequency downshift.

Case (iv) $\epsilon = 0.069$ $(N = 0.30)$

The results are shown in figure 10(*a*, *b*). After a slow start, owing to a small initial wave amplitude, the evolution accelerates and becomes quite chaotic, although the -2nd harmonic clearly becomes dominant toward the end. The amplitude spectrum at $\tau = 45$ also shows a peak at $\nu = -2$.

8.2.3. $u'_*/C = 0.16$

From figure 2(*b*) the equilibrium wave slope is now $(ka)_{\text{eq}} = 0.168$. Initial wave slope $\epsilon = 0.120$ and 0.072 are examined.

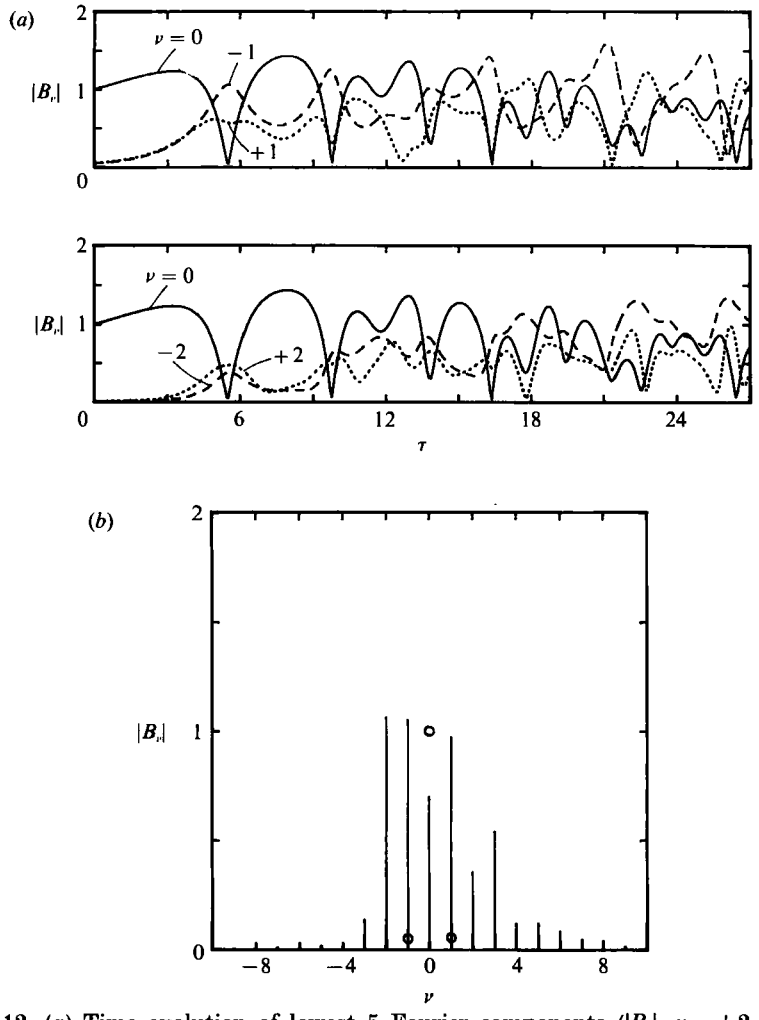

FIGURE 12. (*a*) Time evolution of lowest 5 Fourier components ($|B_\nu|$, $\nu = \pm 2, \pm 1, 0$) of wave amplitude $\tilde{A}$. $u'_*/C = 0.16$, $\epsilon = 0.072$, $K = 1.80$, $\Delta\tau = 0.00063$. (*b*) Amplitude spectrum of wave amplitude $\tilde{A}$ at $\tau = 27$. $u'_*/C = 0.16$, $\epsilon = 0.072$. Circles are spectrum at $\tau = 0$.

Case (v) $\epsilon = 0.120$ $(N = 0.064)$

Since the initial wave amplitude is relatively large, the effect of turbulent dissipation in water (N) is small. The evolution pattern of the lowest 5 harmonics in figure 11 (*a*) is similar to that in case (iii). After many quasi-recurrence cycles, the -1st harmonic gradually outgrows the other harmonics. The final amplitude spectrum in figure 11 (*b*) at $\tau = 75$ clearly shows the permanent frequency downshift.

Case (vi) $\epsilon = 0.072$ $(N = 0.30)$

Because of the relatively small initial wave amplitude and strong wind, the overall spectrum grows rapidly. After the first recurrence cycle, the evolution soon becomes quite chaotic (figure 12*a*). The amplitude spectrum in figure 12 (*b*) at $\tau = 27$ shows that the wave energy is widespread over a broad range of spectrum. We have found that the local maximum wave steepness becomes as large as 0.36. Therefore breaking can take place locally and temporally, which might modify the evolution process. This is unfortunately beyond the scope of our theory.

Based on observations of 6 different cases, we conclude that:

1. Wind plus damping tend to enhance the lower sideband and suppress the upper sideband of the modulational instability, leading to the permanent frequency downshift.

2. If the initial amplitude of the uniform wavetrain is small, higher harmonics of the original sideband instability also become unstable eventually, and the peak frequency tends to migrate further downward.

3. As the wind speed increases, the time evolution becomes more chaotic and the spectrum tends to broaden more rapidly.

The numerical calculations reported here have all been performed with the linear–logarithmic water current profile defined in (2.7). We have also examined the error function current profile, and found qualitatively similar results of the long-time evolution as far as the initial condition is identical.

Based on the numerical results of the evolution of A, we may calculate the time history of the modified surface shear q_0 and the modified induced current ψ^q in (6.60). Then the coefficients κ_{01} and κ_{11} can be calculated in the phase velocity $\tilde{c}$ (6.67) and the group velocity $\tilde{c}_g$ (6.68). However, we recall that in the definition of the basic current profile (2.7), a frame of reference following the surface drift velocity has been chosen. If the logarithmic law is adopted for all depth, then the induced current would become unbounded at $y = -\infty$. In reality the profile eventually deviates from the logarithmic and reaches a constant, whicn in turn defines the real surface drift velocity in the fixed frame of reference. The value of this surface drift must be determined empirically, and is circumvented in this study.

9. Concluding remarks

We have developed a two-dimensional theory for the effect of moderate wind on the long-time evolution of a narrowbanded gravity wave. Eddy viscosity models have been adopted for turbulence in air and water. Energy input from air to water and energy dissipation due to eddy viscosity in water are assumed to occur over the same timescale as the asymmetric evolution of the wave spectrum (fourth-order in wave steepness).

After calculating the nonlinear air flow over gravity waves, the value of the eddy viscosity is determined so that the initial linear growth rate of waves due to wind agrees with Plant's (1982) empirical formula. The nonlinear growth rate decreases as the wave steepness increases, consistent with Gent & Taylor's (1976) second model. Next, we have carried out a perturbation analysis of water waves up to fourth order in wave steepness, and obtained the evolution equation of the wave amplitude $\bar{A}$ and the wave-induced long current $\bar{\psi}_{20}$ on the timescale of $t_3 = \epsilon^3 t$. The effects of the wind energy input, the wind-induced current, and turbulent dissipation in water are all included.

The initial growth rate of sideband instability is found to be sensitive to the assumed profile of wind-induced current in water. The knowledge of the exact current profile is essential to predict the effect of wind accurately. In the subsequent nonlinear evolution of the sideband instability the nonlinear energy input rate from wind through surface normal stress is far more important. With a moderate wind shear the wave energy gradually shifts to the lower sideband, yielding permanent frequency downshift. Although this tendency is present in most of the cases examined, the evolution becomes more chaotic as the wind strength increases.

Our numerical results of the evolution of sideband instability give strong evidence

that the effect of wind can cause the downward migration of the peak frequency of an ocean wave spectrum. However, the present theory is only intended for a weak wind within a narrow range of strength, and does not apply to a stronger wind where breaking may occur. It would be highly desirable to extend our theory to a broadband spectrum on the basis of Zakharov's theory so that more quantitative comparison can be made with laboratory or field observations. However, it appears numerically difficult to compute the nonlinear air flow over such waves. Many formidable challenges are still ahead for a better understanding of physics of wind and waves.

This work was initiated with the support by the Office of Naval Research Physical Oceanography Program under the Accelerated Initiative on Surface Wave Dynamics. Partial support has been received from National Science Foundation Programs of Fluids/Particulates/Hydraulic Systems and Ocean Engineering (Grant no. MSME 8813121).

Appendix A. Simplification of the normal stress boundary condition

First the tangential derivative of (3.13) is taken along the interface:

$$-\frac{\partial p}{\partial x}-\frac{\partial p}{\partial y}\frac{\partial \zeta}{\partial x}+\frac{\partial \zeta}{\partial x}+\sigma_e^2\frac{\partial}{\partial x}(A)+\sigma_e^2\frac{\partial}{\partial y}(A)\frac{\partial \zeta}{\partial x}$$
$$=\frac{\rho'}{\rho}\left[-\frac{\partial p'}{\partial x}-\frac{\partial p'}{\partial y}\frac{\partial \zeta}{\partial x}+\frac{\partial \zeta}{\partial x}+\sigma_e'^2\frac{\partial}{\partial x}(B)+\sigma_e'^2\frac{\partial}{\partial y}(B)\frac{\partial \zeta}{\partial x}\right], \quad \text{(A 1)}$$

where
$$(A)\equiv\left[2\frac{\partial u}{\partial x}n_x n_x+2\frac{\partial v}{\partial y}n_y n_y+2\left(\frac{\partial u}{\partial y}+\frac{\partial v}{\partial x}\right)n_x n_y\right], \quad \text{(A 2)}$$

$$(B)\equiv\left[2\frac{\partial u'}{\partial x}n_x n_x+2\frac{\partial v'}{\partial y}n_y n_y+2\left(\frac{\partial u'}{\partial y}+\frac{\partial v'}{\partial x}\right)n_x n_y\right]. \quad \text{(A 3)}$$

Since the particles on the surface remain there and the velocity is continuous across the surface, we have

$$-\frac{\partial p'}{\partial x}=-\frac{\partial p}{\partial x}+\sigma_e^2\nabla^2 u-\sigma_e'^2\nabla^2 u', \quad \text{(A 4)}$$

$$-\frac{\partial p'}{\partial y}=-\frac{\partial p}{\partial y}+\sigma_e^2\nabla^2 v-\sigma_e'^2\nabla^2 v'. \quad \text{(A 5)}$$

Introducing (A 4) and (A 5) into (A 1) to eliminate p',

$$-\frac{\partial p}{\partial x}-\frac{\partial p}{\partial y}\frac{\partial \zeta}{\partial x}+\frac{\partial \zeta}{\partial x}+\sigma_e^2\frac{\partial}{\partial x}(A)+\sigma_e^2\frac{\partial}{\partial y}(A)\frac{\partial \zeta}{\partial x}=\frac{\rho'}{\rho}\left\{\text{l.h.s.}+\sigma_e^2\nabla^2 u+\sigma_e^2\nabla^2 v\frac{\partial \zeta}{\partial x}\right.$$
$$\left.-\sigma_e^2\frac{\partial}{\partial x}(A)-\sigma_e^2\frac{\partial}{\partial y}(A)\frac{\partial \zeta}{\partial x}-\sigma_e'^2\nabla^2 u'-\sigma_e'^2\nabla^2 v'\frac{\partial \zeta}{\partial x}+\sigma_e'^2\frac{\partial}{\partial x}(B)+\sigma_e'^2\frac{\partial}{\partial y}(B)\frac{\partial \zeta}{\partial x}\right\}. \quad \text{(A 6)}$$

Thus

$$-\frac{\partial p}{\partial x}-\frac{\partial p}{\partial y}\frac{\partial \zeta}{\partial x}+\frac{\partial \zeta}{\partial x}+\sigma_e^2\frac{\partial}{\partial x}(A)+\sigma_e^2\frac{\partial}{\partial y}(A)\frac{\partial \zeta}{\partial x}=\frac{\rho'}{\rho}\left\{\sigma_e^2\nabla^2 u+\sigma_e^2\nabla^2 v\frac{\partial \zeta}{\partial x}-\sigma_e^2\frac{\partial}{\partial x}(A)\right.$$
$$\left.-\sigma_e^2\frac{\partial}{\partial y}(A)\frac{\partial \zeta}{\partial x}-\sigma_e'^2\nabla^2 u'-\sigma_e'^2\nabla^2 v'\frac{\partial \zeta}{\partial x}+\sigma_e'^2\frac{\partial}{\partial x}(B)+\sigma_e'^2\frac{\partial}{\partial y}(B)\frac{\partial \zeta}{\partial x}\right\}\left[1+O\left(\frac{\rho'}{\rho}\right)\right]. \quad \text{(A 7)}$$

Note first that ρ'/ρ is much smaller than the wave slope ϵ of interest. Inside the curly brackets all the terms multiplied by $\sigma_e^2 \sim \epsilon^3$ are negligibly small. Among the terms multiplied by $\sigma_e'^2$, the dominant term is $\sigma_e'^2(\partial^2 u'/\partial y^2)$ from the fifth term in the curly brackets, and all other terms are smaller by a factor of either $O(\epsilon)$ or $O(\delta'^2)$, where δ' is the normalized boundary-layer thickness in air. Based on these observations, the right-hand side of (A 7) is further simplified to:

$$\text{r.h.s. of (A 7)} = -\frac{\rho'\sigma_e'^2}{\rho}\frac{\partial^2 u'}{\partial y^2}[1+O(\epsilon,\delta'^2)] \equiv \frac{\partial f_b'}{\partial x} \tag{A 8}$$

where f_b' is the non-dimensional normal stress due to wind.

Appendix B. Derivation of nonlinear evolution equation of waves at orders 3 and 4

All formulae in this Appendix are deduced with the help of MACSYMA.

At $n = 3$, the forcing terms are found to be

$$F_{30} = -\frac{\partial^3 \psi_{20}}{\partial t_1 \partial y^2}, \tag{B 1}$$

$$F_{31} = -\frac{\partial A}{\partial x_2}e^y - i\frac{\partial^2 A}{\partial x_1 \partial t_1}e^y - \tfrac{1}{2}i\frac{\partial^2 A}{\partial x_1^2}(1-2y)\,e^y + iA\left\{\tfrac{1}{2}e^y\frac{\partial^3 \psi_{20}}{\partial y^3} + g_{00}\frac{\partial^3 \psi^s}{\partial y^3} + \tfrac{1}{2}e^y \times\left[\frac{\partial \psi^s}{\partial y} - \left(\frac{\partial \psi^s}{\partial y}\right)_{y=0}\right]\frac{\partial^3 \psi^s}{\partial y^3}\right\} + \frac{\partial A}{\partial x_1}\left[-2g_{00} + \left(\frac{\partial \psi^s}{\partial y}\right)_{y=0}e^y + \tfrac{1}{2}y\,e^y\frac{\partial^3 \psi^s}{\partial y^3}\right], \tag{B 2}$$

$$F_{32} = -\tfrac{1}{4}iA^2 e^{2y}\frac{\partial^4 \psi^s}{\partial y^4}, \tag{B 3}$$

$$F_{33} = 0, \tag{B 4}$$

$$G_{30} = -\left(\frac{\partial \psi_{20}}{\partial x_1}\right)_{y=0} - \frac{1}{2}\frac{\partial |A|^2}{\partial x_1}, \tag{B 5}$$

$$G_{31} = -\frac{5i}{16}A^2 A^* - \tfrac{1}{2}iA\left(\frac{\partial \psi_{20}}{\partial y}\right)_{y=0} - \frac{1}{2}\frac{\partial A}{\partial x_2} - \tfrac{1}{2}i\frac{\partial^2 A}{\partial x_1^2} - \frac{1}{2}\frac{\partial A}{\partial t_2} - \tfrac{1}{2}i\frac{\partial^2 A}{\partial x_1 \partial t_1}, \tag{B 6}$$

$$G_{32} = -iA^2\left(\frac{1}{4}\frac{\partial^2 \psi^s}{\partial y^2} + \frac{\partial g_{00}}{\partial y}\right)_{y=0} - \tfrac{1}{2}A\frac{\partial A}{\partial x_1}, \tag{B 7}$$

$$G_{33} = -\frac{9i}{16}A^3, \tag{B 8}$$

$$H_{30} = -\left(\frac{\partial^2 \psi_{20}}{\partial y\,\partial t_1}\right)_{y=0} \tag{B 9}$$

$$H_{31} = -iA\left[\frac{1}{2}\frac{\partial \psi^s}{\partial y}\frac{\partial^2 \psi^s}{\partial y^2} - \frac{1}{2}\left(\frac{\partial \psi^s}{\partial y}\right)^2 + \frac{\partial g_{00}}{\partial y}\frac{\partial \psi^s}{\partial y} - \frac{1}{2}\frac{\partial^2 \psi_{20}}{\partial y^2} + \frac{1}{2}\frac{\partial \psi_{20}}{\partial y}\right]_{y=0} - \frac{\partial A}{\partial t_1}\left(\frac{1}{2}\frac{\partial^2 \psi^s}{\partial y^2} - \frac{\partial \psi^s}{\partial y} + \frac{\partial g_{00}}{\partial y}\right)_{y=0} - \frac{1}{2}\left(\frac{\partial \psi^s}{\partial y}\right)_{y=0}\frac{\partial A}{\partial x_1} - \frac{3i}{16}A^2 A^* - \frac{1}{2}\frac{\partial A}{\partial x_2} - \tfrac{1}{2}i\frac{\partial^2 A}{\partial t_1^2} - \frac{1}{2}\frac{\partial A}{\partial t_2}, \tag{B 10}$$

$$H_{32} = -\mathrm{i}A^2\left(\frac{1}{4}\frac{\partial^3\psi^s}{\partial y^3}+\frac{\partial\psi^s}{\partial y}+\frac{\partial g_{00}}{\partial y}\right)_{y=0} - A\frac{\partial A}{\partial t_1}, \tag{B 11}$$

$$H_{33} = \frac{9\mathrm{i}}{16}A^3. \tag{B 12}$$

From (6.27)–(6.29), $F_{30} = G_{30} = H_{30} = 0$. Hence,

$$\psi_{20} = \bar{\psi}_{20}(x_1, x_2, \ldots, y_1, y_2, \ldots, t_1, t_2, \ldots) + \psi^q(x_2, x_3, \ldots, y, t_2, t_3, \ldots), \tag{B 13}$$

$$\frac{\partial\bar{\psi}_{20}}{\partial x_1} = -\frac{1}{2}\frac{\partial|A|^2}{\partial x_1} \quad (y_1 = 0), \tag{B 14}$$

where $\bar{\psi}_{20}$ is the inviscid wave-induced current which depends on slow coordinates only, and ψ^q is the modification to the wind-induced current due to the surface shear q_0 given in (6.60). The former is the consequence of the nonlinear surface kinematic boundary condition and the normal stress boundary condition over long scales.

The solvability condition for ψ_{31} gives

$$\int_{-\infty}^{0} F_{31}\,\mathrm{e}^y\,\mathrm{d}y = H_{31} + G_{31}. \tag{B 15}$$

After introducing (6.41) to eliminate $\partial A/\partial t_1$, we obtain the equation valid for $t_2 = \epsilon^2 t = O(1)$:

$$\frac{\partial A}{\partial t_2}+\frac{1}{2}\frac{\partial A}{\partial x_2}+\tfrac{1}{8}\mathrm{i}\frac{\partial^2 A}{\partial x_1^2}+\tfrac{1}{2}\mathrm{i}|A|^2A+\kappa_{10}\frac{\partial A}{\partial x_1}+\mathrm{i}(\kappa_{01}+\kappa_{20})A = 0, \tag{B 16}$$

where

$$\kappa_{01} = \left(\frac{\partial\psi^q}{\partial y}-\frac{1}{2}\frac{\partial^2\psi^q}{\partial y^2}\right)_{y=0} + \int_{-\infty}^{0}\left(\tfrac{1}{2}\mathrm{e}^{2y}\frac{\partial^3\psi^q}{\partial y^3}\right)\mathrm{d}y, \tag{B 17}$$

$$\kappa_{10} = \frac{1}{2}\left(\frac{\partial\psi^s}{\partial y}\right)_{y=0} + \int_{-\infty}^{0}\left[-2g_{00}+\left(\frac{\partial\psi^s}{\partial y}\right)_{y=0}\mathrm{e}^y+\tfrac{1}{2}y\,\mathrm{e}^y\frac{\partial^3\psi^s}{\partial y^3}\right]\mathrm{e}^y\,\mathrm{d}y, \tag{B 18}$$

$$\kappa_{20} = \frac{1}{8}\left(\frac{\partial^2\psi^s}{\partial y^2}+2\frac{\partial g_{00}}{\partial y}\right)_{y=0}^2 + \int_{-\infty}^{0}\left\{g_{00}\frac{\partial^3\psi^s}{\partial y^3}+\tfrac{1}{2}\mathrm{e}^y\left[\frac{\partial\psi^s}{\partial y}-\left(\frac{\partial\psi^s}{\partial y}\right)_{y=0}\right]\frac{\partial^3\psi^s}{\partial y^3}\right\}\mathrm{e}^y\,\mathrm{d}y. \tag{B 19}$$

The last term in (B 16) is again the modification of phase velocity due to the induced current at $O(\epsilon^2)$, where κ_{01} is due to ψ^q and κ_{20} due to ψ^s. The fifth term in (B 16) is also the consequence of the basic current ψ^s and affects the group velocity at $O(\epsilon)$.

The solutions at $O(\epsilon^3)$ are obtained as

$$\psi_{30} = \psi_{30}(x_1, x_2, \ldots, y, y_1, \ldots, t_1, t_2, \ldots), \tag{B 20}$$

$$\psi_{31} = -\tfrac{5}{16}\mathrm{e}^y A^2A^* + \tfrac{1}{2}\mathrm{i}(1-y)\,\mathrm{e}^y\frac{\partial A}{\partial x_2} - \tfrac{1}{4}(y^2-2y+2)\,\mathrm{e}^y\frac{\partial^2 A}{\partial x_1^2} + \tfrac{1}{2}\mathrm{i}\,\mathrm{e}^y\frac{\partial A}{\partial t_2}$$
$$-\tfrac{1}{2}(1-y)\,\mathrm{e}^y\frac{\partial^2 A}{\partial x_1\,\partial t_1} + \mathrm{i}g_{10}(y)\frac{\partial A}{\partial x_1} + A\left[g_{01}(y)+g_{20}(y)-\frac{1}{2}\left(\frac{\partial\psi^q}{\partial y}\right)_{y=0}\mathrm{e}^y\right], \tag{B 21}$$

$$\psi_{32} = \left[-\frac{\partial g_{30}}{\partial y}+\frac{\partial g_{00}}{\partial y}+\frac{1}{8}\frac{\partial^3\psi^s}{\partial y^3}+\frac{1}{8}\frac{\partial^2\psi^s}{\partial y^2}+\frac{1}{2}\frac{\partial\psi^s}{\partial y}\right]_{y=0}\mathrm{e}^{2y}A^2$$
$$-\tfrac{1}{4}\mathrm{i}\,\mathrm{e}^{2y}A\frac{\partial A}{\partial x_1}-\tfrac{1}{2}\mathrm{i}\,\mathrm{e}^{2y}A\frac{\partial A}{\partial t_1}+g_{30}(y)A^2, \tag{B 22}$$

$$\psi_{33} = 0, \tag{B 23}$$

$$\zeta_{30} = \zeta_{30}(x_1, x_2, \ldots, t_1, t_2, \ldots), \tag{B 24}$$

$$\zeta_{31} = 0, \tag{B 25}$$

$$\zeta_{32} = \left[-\frac{\partial g_{30}}{\partial y} + \frac{3}{2}\frac{\partial g_{00}}{\partial y} + \frac{1}{8}\frac{\partial^3 \psi^s}{\partial y^3} + \frac{1}{4}\frac{\partial^2 \psi^s}{\partial y^2} + \frac{1}{2}\frac{\partial \psi^s}{\partial y}\right]_{y=0} A^2 - \tfrac{1}{2}\mathrm{i}A\frac{\partial A}{\partial x_1} - \tfrac{1}{2}\mathrm{i}A\frac{\partial A}{\partial t_1}, \tag{B 26}$$

$$\zeta_{33} = \tfrac{3}{16}A^3, \tag{B 27}$$

where $g_{01}(y)$, $g_{10}(y)$, $g_{20}(y)$, and $g_{30}(y)$ are the inhomogeneous solutions of the following boundary-value problems

$$\frac{\partial^2 g_{01}}{\partial y^2} - g_{01} = -\tfrac{1}{2}\mathrm{e}^y \frac{\partial^3 \psi^q}{\partial y^3}, \tag{B 28}$$

$$\frac{\partial^2 g_{10}}{\partial y^2} - g_{10} = -2g_{00} + \left(\frac{\partial \psi^s}{\partial y}\right)_{y=0} \mathrm{e}^y + \tfrac{1}{2}y\,\mathrm{e}^y \frac{\partial^3 \psi^s}{\partial y^3}, \tag{B 29}$$

$$\frac{\partial^2 g_{20}}{\partial y^2} - g_{20} = -g_{00}\frac{\partial^3 \psi^s}{\partial y^3} + \frac{1}{2}\left[\left(\frac{\partial \psi^s}{\partial y}\right)_{y=0} - \frac{\partial \psi^s}{\partial y}\right]\mathrm{e}^y \frac{\partial^3 \psi^s}{\partial y^3}, \tag{B 30}$$

$$\frac{\partial^2 g_{30}}{\partial y^2} - 4g_{30} = \tfrac{1}{8}\mathrm{e}^{2y}\frac{\partial^4 \psi^s}{\partial y^4}, \tag{B 31}$$

with boundary conditions

$$g_{01} = g_{10} = g_{20} = g_{30} = 0 \quad (y = 0, -\infty), \tag{B 32}$$

and are obtained numerically. Note that the coefficients κ_{01}, κ_{10} and κ_{20} defined in (B 17) to (B 19) are rewritten as

$$\kappa_{01} = \left(\frac{\partial \psi^q}{\partial y} - \frac{1}{2}\frac{\partial^2 \psi^q}{\partial y^2} + \frac{\partial g_{01}}{\partial y}\right)_{y=0}, \tag{B 33}$$

$$\kappa_{10} = \left(\frac{1}{2}\frac{\partial \psi^s}{\partial y} + \frac{\partial g_{10}}{\partial y}\right)_{y=0}, \tag{B 34}$$

$$\kappa_{20} = \left[\frac{1}{8}\left(\frac{\partial^2 \psi^s}{\partial y^2} + 2\frac{\partial g_{00}}{\partial y}\right)^2 - \frac{\partial g_{20}}{\partial y}\right]_{y=0}. \tag{B 35}$$

At $n = 4$ we only calculate the forcing terms for $m = 1$ to obtain the evolution equation of wave amplitude A in the timescale of $t_3 = \epsilon^2 t = O(1)$:

$$\begin{aligned} F_{41} = {} & \mathrm{i}\left(\tfrac{1}{2}\mathrm{e}^y \frac{\partial^3 \psi_{30}}{\partial y^3} + \tilde{\kappa}_{21} + \tilde{\kappa}_{40}\right)A + \tfrac{5}{4}\mathrm{e}^y AA^*\frac{\partial A}{\partial x_1} + \mathrm{i}\tilde{\kappa}_{60}A^2A^* + \tfrac{5}{8}\mathrm{e}^y A^2\frac{\partial A^*}{\partial x_1} \\ & + (\tilde{\kappa}_{11} + \tilde{\kappa}_{50})\frac{\partial A}{\partial x_1} + \tilde{\kappa}_{10}\frac{\partial A}{\partial x_2} - \mathrm{e}^y\frac{\partial A}{\partial x_3} + \tilde{\kappa}_{70}\frac{\partial A}{\partial t_1} + \mathrm{i}\tilde{\kappa}_{30}\frac{\partial^2 A}{\partial x_1^2} - \mathrm{i}\,\mathrm{e}^y\frac{\partial^2 A}{\partial x_1 \partial x_2} \\ & - \mathrm{i}\,\mathrm{e}^y\frac{\partial^2 A}{\partial x_1 \partial t_2} - \mathrm{i}\,\mathrm{e}^y\frac{\partial^2 A}{\partial x_2 \partial t_1} + \tfrac{1}{2}(y^2 - y + 1)\,\mathrm{e}^y\frac{\partial^3 A}{\partial x_1^3} - \tfrac{1}{2}(2y-1)\,\mathrm{e}^y\frac{\partial^3 A}{\partial x_1^2 \partial t_1}, \end{aligned} \tag{B 36}$$

where

$$\tilde{\kappa}_{11} = -2g_{01} + \left(\frac{\partial \psi^q}{\partial y}\right)_{y=0}\mathrm{e}^y + \tfrac{1}{2}y\,\mathrm{e}^y\frac{\partial^3 \psi^q}{\partial y^3}, \tag{B 37}$$

$$\tilde{\kappa}_{21} = g_{01}\frac{\partial^3 \psi^s}{\partial y^3} + g_{00}\frac{\partial^3 \psi^q}{\partial y^3} + \tfrac{1}{2}\mathrm{e}^y\left[\frac{\partial \psi^q}{\partial y} - \left(\frac{\partial \psi^q}{\partial y}\right)_{y=0}\right]\frac{\partial^3 \psi^s}{\partial y^3} + \tfrac{1}{2}\mathrm{e}^y\left[\frac{\partial \psi^s}{\partial y} - \left(\frac{\partial \psi^s}{\partial y}\right)_{y=0}\right]\frac{\partial^3 \psi^q}{\partial y^3}, \tag{B 38}$$

$$\tilde{\kappa}_{10} = -2g_{00} + \tfrac{1}{2}y\,\mathrm{e}^{y}\frac{\partial^3\psi^{\mathrm{s}}}{\partial y^3} + \mathrm{e}^{y}\left(\frac{\partial\psi^{\mathrm{s}}}{\partial y}\right)_{y=0}, \tag{B 39}$$

$$\tilde{\kappa}_{30} = -\frac{1}{4}\left[8g_{10} - 4g_{00} + y^2\,\mathrm{e}^{y}\frac{\partial^3\psi^{\mathrm{s}}}{\partial y^3} + 2\mathrm{e}^{y}\left(\frac{\partial\psi^{\mathrm{s}}}{\partial y}\right)_{y=0}\right], \tag{B 40}$$

$$\tilde{\kappa}_{40} = \frac{\partial^3\psi^{\mathrm{s}}}{\partial y^3}\left[g_{20} + g_{00}\frac{\partial\psi^{\mathrm{s}}}{\partial y} - \tfrac{1}{2}\mathrm{e}^{y}\frac{\partial\psi^{\mathrm{s}}}{\partial y}\left(\frac{\partial\psi^{\mathrm{s}}}{\partial y}\right)_{y=0} + \tfrac{1}{2}\mathrm{e}^{y}\left(\frac{\partial\psi^{\mathrm{s}}}{\partial y}\right)^2\right], \tag{B 41}$$

$$\tilde{\kappa}_{50} = -2g_{20} - \frac{1}{2}\frac{\partial^3\psi^{\mathrm{s}}}{\partial y^3}\left\{2g_{10} - 2g_{00} - y\,\mathrm{e}^{y}\frac{\partial\psi^{\mathrm{s}}}{\partial y} + \left[\left(\frac{\partial\psi^{\mathrm{s}}}{\partial y}\right)_{y=0} - \frac{\partial\psi^{\mathrm{s}}}{\partial y}\right]\mathrm{e}^{y}\right\}, \tag{B 42}$$

$$\tilde{\kappa}_{60} = -\tfrac{1}{16}\mathrm{e}^{3y}\frac{\partial^5\psi^{\mathrm{s}}}{\partial y^5} - \tfrac{1}{4}\mathrm{e}^{3y}\frac{\partial^4\psi^{\mathrm{s}}}{\partial y^4} - \tfrac{5}{16}\mathrm{e}^{y}\frac{\partial^3\psi^{\mathrm{s}}}{\partial y^3}, \tag{B 43}$$

$$\tilde{\kappa}_{70} = \frac{1}{2}\frac{\partial^3\psi^{\mathrm{s}}}{\partial y^3}\left\{2g_{00} - \left[\left(\frac{\partial\psi^{\mathrm{s}}}{\partial y}\right)_{y=0} - \frac{\partial\psi^{\mathrm{s}}}{\partial y}\right]\mathrm{e}^{y}\right\}, \tag{B 44}$$

and

$$\begin{aligned} G_{41} = &-\left[\tfrac{1}{2}\mathrm{i}\left(\frac{\partial\bar{\psi}_{20}}{\partial y_1}\right)_{y_1=0} + \tfrac{1}{2}\mathrm{i}\left(\frac{\partial\psi_{30}}{\partial y}\right)_{y=0} + \tfrac{1}{2}\mathrm{i}\zeta_{20} + N\right]A - \tfrac{5}{8}AA^*\frac{\partial A}{\partial t_1} \\ &- \tfrac{5}{8}AA^*\frac{\partial A}{\partial x_1} + \mathrm{i}\left(\frac{\partial g_{30}}{\partial y} - 2\frac{\partial g_{00}}{\partial y} - \frac{1}{16}\frac{\partial^3\psi^{\mathrm{s}}}{\partial y^3} - \frac{3}{8}\frac{\partial^2\psi^{\mathrm{s}}}{\partial y^2} - \frac{7}{16}\frac{\partial\psi^{\mathrm{s}}}{\partial y}\right)_{y=0}A^2A^* \\ &- \tfrac{3}{16}A^2\frac{\partial A^*}{\partial t_1} + \tfrac{1}{16}A^2\frac{\partial A^*}{\partial x_1} - \frac{1}{2}\frac{\partial A}{\partial x_3} - \frac{1}{2}\frac{\partial A}{\partial t_3} - \mathrm{i}\frac{\partial^2 A}{\partial x_1\,\partial x_2} \\ &- \tfrac{1}{2}\mathrm{i}\frac{\partial^2 A}{\partial x_1\,\partial t_2} - \tfrac{1}{2}\mathrm{i}\frac{\partial^2 A}{\partial x_2\,\partial t_1} + \frac{1}{2}\frac{\partial^3 A}{\partial x_1^3} + \frac{1}{2}\frac{\partial^3 A}{\partial x_1^2\,\partial t_1}, \end{aligned} \tag{B 45}$$

$$\begin{aligned} H_{41} = &-\mathrm{i}\left[\frac{1}{2}\frac{\partial\psi^{q}}{\partial y}\frac{\partial^2\psi^{\mathrm{s}}}{\partial y^2} + \frac{1}{2}\frac{\partial\psi^{\mathrm{s}}}{\partial y}\frac{\partial^2\psi^{q}}{\partial y^2} - \frac{\partial\psi^{\mathrm{s}}}{\partial y}\frac{\partial\psi^{q}}{\partial y} + \frac{\partial g_{01}}{\partial y}\frac{\partial\psi^{\mathrm{s}}}{\partial y} + \frac{\partial g_{00}}{\partial y}\frac{\partial\psi^{q}}{\partial y} - \frac{1}{2}\frac{\partial^2\psi_{30}}{\partial y^2} + \frac{1}{2}\frac{\partial\psi_{30}}{\partial y}\right]_{y=0}A \\ &- \left(\frac{1}{2}\frac{\partial^2\psi^{q}}{\partial y^2} - \frac{\partial\psi^{q}}{\partial y} + \frac{\partial g_{01}}{\partial y}\right)_{y=0}\frac{\partial A}{\partial t_1} + \frac{1}{2}\left[\mathrm{i}\zeta_{20} - 2\mathrm{i}\left(\frac{\partial\psi^{\mathrm{s}}}{\partial y}\frac{\partial g_{20}}{\partial y}\right)_{y=0} + \left(\frac{\partial\bar{\psi}_{20}}{\partial x_1}\right)_{y_1=0} - 2N\right. \\ &\left. - \mathrm{i}\left(\frac{\partial\bar{\psi}_{20}}{\partial y_1}\right)_{y_1=0}\right]A - \tfrac{1}{16}\mathrm{i}\left(16\frac{\partial g_{30}}{\partial y} - 2\frac{\partial g_{00}}{\partial y} + \frac{\partial^4\psi^{\mathrm{s}}}{\partial y^4} - \frac{\partial^3\psi^{\mathrm{s}}}{\partial y^3} + 6\frac{\partial^2\psi^{\mathrm{s}}}{\partial y^2} - 15\frac{\partial\psi^{\mathrm{s}}}{\partial y}\right)_{y=0}A^2A^* \\ &+ \frac{1}{2}\left[\frac{\partial\psi^{\mathrm{s}}}{\partial y}\left(2\frac{\partial g_{10}}{\partial y} - 2\frac{\partial g_{00}}{\partial y} - \frac{\partial^2\psi^{\mathrm{s}}}{\partial y^2} + \frac{\partial\psi^{\mathrm{s}}}{\partial y}\right) - \frac{\partial\psi^{q}}{\partial y}\right]_{y=0}\frac{\partial A}{\partial x_1} + \tfrac{9}{8}AA^*\frac{\partial A}{\partial t_1} - \tfrac{1}{4}AA^*\frac{\partial A}{\partial x_1} \\ &+ \tfrac{3}{16}A^2\frac{\partial A^*}{\partial t_1} - \frac{1}{2}\left(\frac{\partial\psi^{\mathrm{s}}}{\partial y}\right)_{y=0}\frac{\partial A}{\partial x_2} - \frac{1}{2}\frac{\partial A}{\partial x_3} - \left(\frac{\partial g_{20}}{\partial y}\right)_{y=0}\frac{\partial A}{\partial t_1} - \frac{1}{2}\left(2\frac{\partial g_{00}}{\partial y} + \frac{\partial^2\psi^{\mathrm{s}}}{\partial y^2}\right. \\ &\left. - 2\frac{\partial\psi^{\mathrm{s}}}{\partial y}\right)_{y=0}\frac{\partial A}{\partial t_2} - \frac{1}{2}\frac{\partial A}{\partial t_3} - \tfrac{1}{2}\mathrm{i}\left(2\frac{\partial g_{10}}{\partial y} + \frac{\partial\psi^{\mathrm{s}}}{\partial y}\right)_{y=0}\frac{\partial^2 A}{\partial x_1\,\partial t_1} - \mathrm{i}\frac{\partial^2 A}{\partial t_1\,\partial t_2} + Np_1. \end{aligned} \tag{B 46}$$

The solvability condition for ψ_{41} gives

$$\int_{-\infty}^{0} F_{41}\,\mathrm{e}^{y}\,\mathrm{d}y = H_{41} + G_{41}. \tag{B 47}$$

After invoking (6.41), (B 14), and (B 16), we obtain the evolution equation of A over the timescale of $t_3 = \epsilon^3 t$:

$$\frac{\partial A}{\partial t_3}+\frac{1}{2}\frac{\partial A}{\partial x_3}-\frac{1}{16}\frac{\partial^3 A}{\partial x_1^3}+\tfrac{1}{4}\mathrm{i}\frac{\partial^2 A}{\partial x_1 \partial x_2}+\tfrac{3}{2}AA^*\frac{\partial A}{\partial x_1}+\tfrac{1}{4}A^2\frac{\partial A^*}{\partial x_1}+\mathrm{i}\left(\frac{\partial \bar{\psi}_{20}}{\partial y_1}\right)_{y_1=0}A+2NA+\mathrm{i}\kappa_{30}\frac{\partial^2 A}{\partial x_1^2}$$

$$+\kappa_{10}\frac{\partial A}{\partial x_2}+\mathrm{i}\kappa_{60}|A|^2A+\mathrm{i}(\kappa_{02}+\kappa_{21}+\kappa_{40})A+(\kappa_{11}+\kappa_{50})\frac{\partial A}{\partial x_1}-Np_1=0, \quad \text{(B 48)}$$

where

$$\kappa_{02}=\left(\frac{\partial \psi_{30}}{\partial y}-\frac{1}{2}\frac{\partial^2 \psi_{30}}{\partial y^2}\right)_{y=0}+\int_{-\infty}^{0}\left(\tfrac{1}{2}\mathrm{e}^{2y}\frac{\partial^3 \psi_{30}}{\partial y^3}\right)\mathrm{d}y, \quad \text{(B 49)}$$

$$\kappa_{11}=\frac{1}{2}\left(\frac{\partial \psi^q}{\partial y}\right)_{y=0}+\int_{-\infty}^{0}\left[-2g_{01}+\left(\frac{\partial \psi^q}{\partial y}\right)_{y=0}\mathrm{e}^y+\tfrac{1}{2}y\,\mathrm{e}^y\frac{\partial^3 \psi^q}{\partial y^3}\right]\mathrm{e}^y\,\mathrm{d}y, \quad \text{(B 50)}$$

$$\kappa_{21}=\frac{1}{4}\left(\frac{\partial^2 \psi^s}{\partial y^2}+2\frac{\partial g_{00}}{\partial y}\right)_{y=0}\left(\frac{\partial^2 \psi^q}{\partial y^2}+2\frac{\partial g_{01}}{\partial y}\right)_{y=0}+\int_{-\infty}^{0}\left\{g_{01}\frac{\partial^3 \psi^s}{\partial y^3}+g_{00}\frac{\partial^3 \psi^q}{\partial y^3}\right.$$

$$\left.+\tfrac{1}{2}\mathrm{e}^y\left[\frac{\partial \psi^q}{\partial y}-\left(\frac{\partial \psi^q}{\partial y}\right)_{y=0}\right]\frac{\partial^3 \psi^s}{\partial y^3}+\tfrac{1}{2}\mathrm{e}^y\left[\frac{\partial \psi^s}{\partial y}-\left(\frac{\partial \psi^s}{\partial y}\right)_{y=0}\right]\frac{\partial^3 \psi^q}{\partial y^3}\right\}\mathrm{e}^y\,\mathrm{d}y, \quad \text{(B 51)}$$

$$\kappa_{30}=\int_{-\infty}^{0}\tilde{\kappa}_{30}\,\mathrm{e}^y\,\mathrm{d}y \quad \text{(B 52)}$$

$$\kappa_{40}=\left(\frac{\partial g_{00}}{\partial y}\frac{\partial g_{20}}{\partial y}+\frac{1}{2}\frac{\partial^2 \psi^s}{\partial y^2}\frac{\partial g_{20}}{\partial y}\right)_{y=0}+\int_{-\infty}^{0}\tilde{\kappa}_{40}\,\mathrm{e}^y\,\mathrm{d}y$$

$$+\left(\frac{\partial g_{00}}{\partial y}+\frac{1}{2}\frac{\partial^2 \psi^s}{\partial y^2}-\frac{\partial \psi^s}{\partial y}\right)_{y=0}\int_{-\infty}^{0}\tilde{\kappa}_{70}\,\mathrm{e}^y\,\mathrm{d}y, \quad \text{(B 53)}$$

$$\kappa_{50}=-\frac{1}{16}\left(\frac{\partial^2 \psi^s}{\partial y^2}+2\frac{\partial g_{00}}{\partial y}\right)_{y=0}\left[8\left(\frac{\partial g_{10}}{\partial y}-\frac{1}{2}\frac{\partial \psi^s}{\partial y}\right)+\left(\frac{\partial^2 \psi^s}{\partial y^2}+2\frac{\partial g_{00}}{\partial y}\right)\right]_{y=0}$$

$$-\frac{1}{2}\int_{-\infty}^{0}\tilde{\kappa}_{70}\,\mathrm{e}^y\,\mathrm{d}y+\int_{-\infty}^{0}\tilde{\kappa}_{50}\,\mathrm{e}^y\,\mathrm{d}y, \quad \text{(B 54)}$$

$$\kappa_{60}=\frac{1}{16}\left(\frac{\partial^4 \psi^s}{\partial y^4}+8\frac{\partial^2 \psi^s}{\partial y^2}+22\frac{\partial g_{00}}{\partial y}\right)_{y=0}+\int_{-\infty}^{0}\tilde{\kappa}_{60}\,\mathrm{e}^y\,\mathrm{d}y, \quad \text{(B 55)}$$

and $\tilde{\kappa}_{30} \sim \tilde{\kappa}_{70}$ are defined by (B 40) $\sim$ (B 44).

In the evolution equation (B 48) all the κ are the effects of the induced current ψ^s, ψ^q, and ψ_{30}. The phase velocity is modified by κ_{02}, κ_{21}, and κ_{40} at $O(\epsilon^3)$, and the group velocity is modified by κ_{11} and κ_{50} at $O(\epsilon^2)$. At this order ψ^s also affects the nonlinear dispersion through κ_{60} and the linear dispersion through κ_{30}. The effects of the normal wind stress p_1 appears at this order through the surface boundary condition (6.19).

By combining (6.41), (B 16) and (B 48), we obtain the evolution equation up to $\epsilon^3 t = O(1)$:

$$\frac{\partial A}{\partial t_1}+[\tfrac{1}{2}+\epsilon\kappa_{10}+\epsilon^2(\kappa_{11}+\kappa_{50})]\frac{\partial A}{\partial x_1}+\mathrm{i}[\kappa_{00}+\epsilon(\kappa_{01}+\kappa_{20})$$

$$+\epsilon^2(\kappa_{02}+\kappa_{21}+\kappa_{40})]A+\mathrm{i}(\tfrac{1}{8}\epsilon+\epsilon^2\kappa_{30})\frac{\partial^2 A}{\partial x_1^2}+\mathrm{i}(\tfrac{1}{2}\epsilon+\epsilon^2\kappa_{60})|A|^2A-\tfrac{1}{16}\epsilon^2\frac{\partial^3 A}{\partial x_1^3}$$

$$+\tfrac{3}{2}\epsilon^2|A|^2\frac{\partial A}{\partial x_1}+\tfrac{1}{4}\epsilon^2A^2\frac{\partial A^*}{\partial x_1}+\epsilon^2\,\mathrm{i}\left(\frac{\partial \bar{\psi}_{20}}{\partial y_1}\right)_{y_1=0}A+\epsilon^2 2NA-\epsilon^2 Np_1=0. \quad \text{(B 56)}$$

At $O(\epsilon^5)$ we obtain the forcing term F_{50} in the limit of $y \to -\infty$ as

$$F_{50} = \left(\frac{\partial^2}{\partial x_1^2} + \frac{\partial^2}{\partial y_1^2}\right)\frac{\partial \bar{\psi}_{20}}{\partial t_1}. \tag{B 57}$$

Therefore $\bar{\psi}_{20}$ is governed by the Laplace equation in long scales:

$$\frac{\partial^2 \bar{\psi}_{20}}{\partial x_1^2} + \frac{\partial^2 \bar{\psi}_{20}}{\partial y_1^2} = 0, \tag{B 58}$$

with the surface boundary condition (B 14) and

$$\bar{\psi}_{20} = 0, \quad y_1 = -\infty. \tag{B 59}$$

Equation (B 56) together with (B 58), (B 59), (B 14) constitute the evolution equations of the wave amplitude A and the wave induced current $\bar{\psi}_{20}$ up to $\epsilon^3 t = O(1)$.

REFERENCES

Banner, M. L. & Melville, W. K. 1976 On the separation of air flow over water waves. *J. Fluid Mech.* **77**, 825–842.

Banner, M. L. & Phillips, O. M. 1974 On the incipient breaking of small scale waves. *J. Fluid Mech.* **65**, 647–656.

Blennerhassett, P. J. 1980 On the generation of waves by wind. *Phil. Trans. R. Soc. Lond.* A **298**, 451–494.

Bliven, L. F., Huang, N. E. & Long, S. R. 1986 Experimental study of the influence of wind on Benjamin–Feir sideband instability. *J. Fluid Mech.* **162**, 237–260.

Caponi, E. A., Fornberg, B., Knight, D. D., Mclean, J. W., Saffman, P. G. & Yuen, H. C. 1982 Calculation of laminar viscous flow over a moving wavy surface. *J. Fluid Mech.* **124**, 347–362.

Charnock, H. 1955 Wind stress on a water surface. *Q. J. R. Met. Soc.* **81**, 639–642.

Dhar, A. K. & Das, K. P. 1990 A fourth-order evolution equation for deep water surface gravity waves in the presence of wind blowing over water. *Phys. Fluids* A **2**, 778–783.

Dysthe, K. B. 1979 Note on a modification to the nonlinear Schrödinger equation for application to deep water waves. *Proc. R. Soc. Lond.* A **369**, 105–114.

Gent, P. R. & Taylor, P. A. 1976 A numerical model of the air flow above water waves. *J. Fluid Mech.* **77**, 105–128.

Hasselmann, K. *et al.* 1973 Measurements of wind wave growth and swell decay during the Joint North Sea Wave Project (jonswap). *Herausgegeben vom Deutsch. Hydrogr. Institut.* A, no. 12, 95 pp.

Jacobs, S. J. 1987 An asymptotic theory for the turbulent flow over a progressive water wave. *J. Fluid Mech.* **174**, 69–80.

Janssen, P. A. E. M. 1986 The periodic-doubling of gravity–capillary waves. *J. Fluid Mech.* **172**, 531–546.

Kawai, S. 1979 Generation of initial wavelets by instability of a coupled shear flow and their evolution to wind waves. *J. Fluid Mech.* **93**, 661–703.

Lake, B. M., Yuen, H. C., Rungaldier, H. & Ferguson, I. N. E. 1977 Nonlinear deep water waves: Theory and experiment. Part 2. Evolution of a continuous wave train. *J. Fluid Mech.* **83**, 49–74.

Larson, T. R. & Wright, J. W. 1975 Wind-generated gravity–capillary waves: laboratory measurements of temporal growth rates using microwave backscatter. *J. Fluid Mech.* **70**, 417–436.

Li, J. C., Hui, W. H. & Donelan, M. A. 1987 Effects of velocity shear on the stability of surface deep water wave trains. In *Nonlinear Water Waves (IUTAM Symposium)*, pp. 213–220. Springer.

Lo, E. & Mei, C. C. 1985 A numerical study of water-wave modulation based on a higher-order nonlinear Schrödinger equation. *J. Fluid Mech.* **150**, 395–416.

Longuet-Higgins, M. S. & Turner, J. S. 1985 An 'entraining plume' model of a spilling breaker. *J. Fluid Mech.* **63**, 1–20.

Melville, W. K. 1982 The instability and breaking of deep-water waves. *J. Fluid Mech.* **115**, 165–185.

Miles, J. W. 1957 On the generation of surface waves by shear flows. *J. Fluid Mech.* **3**, 185–204.

Mitsuyasu, H. & Honda, T. 1982 Wind-induced growth of water waves. *J. Fluid Mech.* **123**, 425–442.

Pierson, W. J., Neuman, G. & James, R. W. 1958 Practical methods for observing and forecasting ocean waves by means of wave spectra and statistics. Hydrographic office, US Navy.

Plant, W. J. 1982 A relationship between wind stress and wave slope. *J. Geophys. Res.* **87**, 1961–1967.

Plant, W. J. 1990 Wave influences on wind profiles over water. Submitted for publication.

Schlichting, H. 1955 *Boundary-Layer Theory*. McGraw-Hill.

Shemdin, O. H. & Hsu, E. Y. 1967 Direct measurements of aerodynamic pressure above a simple progressive gravity wave. *J. Fluid Mech.* **30**, 403–416.

Snyder, R. L., Dobson, F. W., Elliott, J. A. & Long, R. B. 1981 Array measurements of atmospheric pressure fluctuations above surface gravity waves. *J. Fluid Mech.* **102**, 1–59.

Stewart, R. W. 1974 The air–sea momentum exchange. *Boundary-Layer Met.* **6**, 151–167.

Townsend, A. A. 1972 Flow in a deep turbulent boundary layer over a surface distorted by water waves. *J. Fluid Mech.* **55**, 719–735.

Trulsen, K. & Dysthe, K. B. 1989 Frequency down-shift through self modulation and breaking. *Water Wave Kinematics*, NATO ASI series. Kluwer.

Valenzuela, G. R. 1976 The growth of gravity–capillary waves in a coupled shear flow. *J. Fluid Mech.* **76**, 229–250.

Yuen, H. C. & Lake, B. M. 1982 Nonlinear dynamics of deep water gravity waves. *Adv. Appl. Mech.* **22**, 67–229.

Wu, H. Y., Hsu, E. Y. & Street, R. L. 1977 The energy transfer due to air-input, non-linear wave–wave interaction and white cap dissipation associated with wind-generated waves. *Tech. Rep.* 207, pp. 1–158. Stanford University.

Wu, H. Y., Hsu, E. Y. & Street, R. L. 1979 Experimental study of non-linear wave–wave interaction and white-cap dissipation of wind-generated waves. *Dyn. Atmos. Oceans* **3**, 55–78.

Wu, J. 1975 Wind-induced drift currents. *J. Fluid Mech.* **68**, 49–70.